Converted Measurements Bayesian Extended Target Tracking Applied to X-band Marine Radar Data

GEMINE VIVONE
PAOLO BRACA
KARL GRANSTRÖM
ANTONIO NATALE
JOCELYN CHANUSSOT

X-band marine radar systems are flexible and low-cost tools for monitoring multiple targets in a surveillance area. They can provide high resolution measurements both in space and time. Such features offer the opportunity to get accurate information not only about the target kinematics, as other conventional sensors, but also about the target size.

In this paper we exploit the random matrix framework to track extended targets. Proper measurement models to deal with the radar's measurement noise and its conversion into Cartesian coordinates are presented here. Benefits of the proposed extended target tracking using converted measurements can be mainly related to the problem of the targets' size estimation, while advantages on estimation of the targets' kinematic features can be considered negligible. The validity of the proposed approach has been demonstrated by using both simulated and real data. Gains up to 70% for the targets' width estimation accuracy and around 65% for the length are observed on real data. The integration of the proposed model into the gamma Gaussian inverse Wishart probability hypothesis density tracker is also provided and tested on real data.

Manuscript received December 18, 2015; revised July 8, 2016; released for publication July 22, 2016.

Refereeing of this contribution was handled by Dr. Marcus Baum.

Authors' addresses: G. Vivone and P. Braca are with the North Atlantic Treaty Organization (NATO) Science and Technology Organization (STO) Centre for Maritime Research and Experimentation, 19126 La Spezia, Italy (E-mail: {gemine.vivone,paolo.braca}@cmre.nato.int). K. Granström is with the Department of Signals and Systems, Chalmers University of Technology, Gothenburg, 412 96, Sweden (E-mail: karl.granstrom@chalmers.se). A. Natale is with IREA-CNR, Napoli, Italy (E-mail: natale.a@irea.cnr.it). J. Chanussot is with the Grenoble Images Speech Signals and Automatics Laboratory (GIPSA-Lab), Grenoble Institute of Technology, 38000 Grenoble, France, and also with the Faculty of Electrical and Computer Engineering, University of Iceland, 107 Reykjavík, Iceland. (E-mail: jocelyn.chanussot@gipsa-lab.grenoble-inp.fr).

The authors declare no conflict-of-interest.

I. INTRODUCTION

Securing the waterways is of critical importance, and surveillance activities take on a central role. Ship traffic monitoring and port protection represent big challenges (e.g. in terms of law enforcement, search and rescue, environmental protection, and resource management) and, in the last years, it has stimulated intensive research activities, e.g. [9], [22], [31], [41].

Radars are widely exploited technologies. Among these, X-band marine radar systems represent flexible and low-cost tools for tracking of multiple targets. Features, such as high resolution in both space and time, make these kinds of systems very appealing because, if compared to conventional radars, they are able to provide indications about the targets' size and not only about targets' kinematics. This additional information can be very helpful for subsequent signal processing phases, e.g. target classification.

The tracking literature is mostly focused on approaches that make the hypothesis of at most one detection per target for each frame, see for instance [3], [7], [28], [31], [41], which is no longer valid for the data considered in this paper. We refer to this problem as *extended target tracking* (ETT). Several approaches can be found in the literature to address the ETT problem.

Bar-Shalom, et al. [3] propose to segment the acquired image. Clustering and centroid extraction phases are subsequently used to provide data for feeding the probabilistic data association (PDA) algorithm. A technique for data association using a multi-assignment approach to track a large number of closely spaced (and overlapping) targets is also presented in [24]. In [14], the authors propose an approach for ETT under the assumption that the number of received measurements is a Poisson distribution. The algorithm is illustrated with point targets, which may generate more than one measurement and have a 1-D extension. A sequential Monte Carlo method is also proposed in [13], where sensor measurements are modeled as a Poisson process with a spatially dependent intensity parameter, which leads to the representation of physical extent as an intensity distribution that avoids the evaluation of explicit data association hypotheses. A similar approach is taken in [8] where track-before-detect theory is used to track a point target with a 1-D extent. The application of track-before-detect theory together with particle filters on X-band marine radar data has also been investigated in [11]. An interacting multiple model data augmentation algorithm and a modified version of the mixture Kalman filter are proposed for extended target tracking in [2]. Two models, based on support functions for smooth object shapes and extended Gaussian image in the non-smooth object case, are proposed and used for extended target tracking in [39]. In [34] the problem of group structure inference and joint detection and tracking for group and individual targets within a

Bayesian filtering framework is addressed. Group dynamical models from a continuous time setting, the interaction models for closely spaced targets, and a group structure transition model are proposed. Baum, et al. introduce in [5], [6] the random hypersurface model for estimating both kinematic and shape parameters of extended targets. Specific estimators are derived for elliptic and star-convex shapes. In [30], Mahler proposes an expansion to extended targets of his probability hypothesis density filter [29] to manage the multi-target tracking problem. Unfortunately, the proposed filter requires processing of all possible measurement set partitions, which is generally unfeasible to implement. An approach for limiting the number of considered partitions is proposed and discussed in [20]. A sequential Monte Carlo multi-target Bayes filter based on finite set statistics is exploited for pedestrian tracking in [35]. Furthermore, a nonlinear Bayesian methodology for image sequences incorporating the statistical models for the background clutter, target motion, and target aspect change is proposed in [10].

A popular and computationally efficient framework to handle this issue, under the hypothesis of elliptical spread of the target, is provided by Koch in [25] where an approximate Bayesian solution to the target tracking problem is proposed. Random matrices are exploited to model the ellipsoidal object extensions, which are treated as additional state variables to be estimated or tracked. The target kinematic states are modeled using a Gaussian distribution, while the ellipsoidal target extension is modeled using an inverse Wishart distribution. Random matrices are used to model extended targets under kinematic constraints [26]. In [45], [46] and [19], the integration of random matrices into the probabilistic multi-hypothesis tracking and the probability hypothesis density filter, respectively, address the multi-target tracking problem. Furthermore, a new approach is derived in [12] to overcome some of the weaknesses in [25]. Indeed, in [25] sensor inaccuracies are neglected and, if they are large in comparison to target size, the lack of modeling may lead to an overestimation of target size, see [11]. New measurement and time updates for [12] are proposed in [33] and [21], respectively. An extension of random matrices for non-ellipsoidal group and extended target tracking based on a combination of multiple ellipsoidal sub-objects, each represented by a random matrix, is discussed in [27]. A comparison between random matrices and the random hypersurface model [5] under a single target assumption is given in [4]. An interesting application using real-world radar data, acquired during the recovery operations of the Costa Concordia wreckage in October 2013, and the random matrices framework is reported in [16], [17].

An overview of the state-of-art for group and extended target tracking techniques is given in [32]. Sequential Monte Carlo methods and their variants are mainly discussed. An overview including Markov chain Monte Carlo (MCMC) methods, random matrices approaches, and random finite set statistics techniques is also provided.

In radar signal processing a crucial point is given by the data conversion. The measurement of the target's position is usually reported in polar coordinates, while the target position and dynamic are usually modeled in Cartesian coordinates. The effects of data conversion have to be properly taken into consideration.

In this paper, we propose to investigate further the conversion between polar and Cartesian coordinates into the approach presented in [12]. An extended target tracking algorithm is presented here and two measurement models using two kinds of coordinate conversions (i.e. the standard and the unbiased ones) are illustrated and integrated into the random matrix framework. Sects. II-C and III-B show the proposed models and how it is possible to integrate them into the random matrix framework. Furthermore, we derive that the update equations are similar to the ones in [12]. Estimations for both kinematic parameters (i.e. positions and velocities) and sizes are performed. The performance of the proposed models are assessed on both simulated data (reproducing three different scenarios) and real data acquired by an X-band marine radar installed in the Gulf of La Spezia, Italy. Comparisons with the measurement model that neglects the sensors' noise effects (e.g. [25]) and the one with a constant covariance matrix [12] are provided. Automatic identification system (AIS) static and kinematic reports are exploited as ground truth in order to assess the performance. The simulation results are confirmed by real data. Ten different target datasets exploiting different kinds of targets, with over 10^3 frames of acquisition, are used to obtain a significant statistical analysis. It is demonstrated that the main advantage is the improvement in the estimation of target size, while comparable performance can be shown on the estimation of kinematic parameters. More specifically, gains up to 70% for the targets' width estimation accuracy and 65% for the length are observed by exploiting the proposed models. The integration of the proposed model into the gamma Gaussian inverse Wishart probability hypothesis density tracker [17] to address real scenarios with clutter and expected multiple extended targets is also provided and tested on real data. To the best of the authors' knowledge, this represents the first attempt to integrate the coordinate conversion into the random matrix framework and to quantitatively evaluate the effects of the sensors' noise and data conversion in ETT using both simulated and X-band marine radar data. Indeed, even if other few performance assessments relied upon these data can be found in the literature, see [11], [17], a serious analysis on the effects of the sensors' noise has not been accounted for.

Furthermore, the problem of dealing with nonlinearities is of great interest in radar signal processing

especially because these strategies risk to fail in specific cases and ad hoc improvements need to be implemented, see e.g. [37]. This is also the case of the proposed paper, in which the non-linearity problem (conversion of data) is completely neglected for the ETT literature, which has attracted great interest in the recent years. The impact in neglecting the noise and its conversion between polar and Cartesian coordinates is particularly clear, see Sect. V, on the target's size estimation. Nowadays, many papers propose its own extended target tracking approach and these techniques are increasing interest thanks to the high resolution features of several new radar systems. However, all these approaches neglect the polar-Cartesian conversion issue causing a bias in the estimation of the targets' extension. Thus, new researches can arise from this paper integrating the conversion in these approaches and by evaluating the benefits on real radar data. The contribute of the paper is twofold:

- **Theoretical.** We derive first the *converted measurement extended target tracking* (CM-ETT), which represents the extension of the converted measurement Kalman filter to the context of extended targets, see Sects. II-C and III. Furthermore, the similarities with respect to the work of Feldmann et al. [12] are remarked. Similar update equations can be derived but exploiting a state-dependent covariance noise matrix.
- **Experimental.** We show that the CM-ETT significantly outperforms the ETT state-of-the-art strategies by validating it in extensive experiments, that is hardly to find in this literature. Several simulated scenarios have been tested quantifying the benefits in using the proposed model. Furthermore, the use of 10 real datasets including data from several kinds of targets, acquired by our X-band marine radar in the Gulf of La Spezia, together with the AIS information enables us to further corroborate the simulated outcomes on real data. The integration with the multiple extended target strategy in [17] is also provided and validated on a challenging real data set.

The work presented in this paper is an extension of previously reported progress on ETT applied to X-band marine radar data [40]. A broader experimental analysis, a more detailed analysis of the literature, the introduction of the unbiased coordinate conversion, and the extension to the multiple ETT case integrating the proposed converted measurement model into the gamma Gaussian inverse Wishart probability hypothesis density tracker [17] validating it on real data, can be considered the main novelties of this paper with respect to the conference version.

The paper is organized as follows. Sect. II describes the Bayesian extended target modeling, including a coordinate conversion model approach. Sect. III presents the filtering equations that the modeling lead to. Sect. IV is devoted to the integration of the proposed approach into the gamma Gaussian inverse Wishart probability hypothesis density tracker. The experimental results using both simulated and real data are shown in Sect. V. Results in the multiple extended target tracking case are presented in Sect. VI. Finally, conclusions and future developments are drawn in Sect. VII.

II. BAYESIAN EXTENDED TARGET MODELING

This section is devoted to the description of the proposed measurement model using converted measurements and its integration into the Bayesian extended target tracking framework presented first in [25], and later improved in [12] with the consideration of the sensors' measurement errors. It is worth pointing out that the above-mentioned papers concentrate attention on the track filtering. Estimations under observation-to-track association uncertainty with possible presence of missed detections and false alarms are out-of-scope. The same assumption is made in this paper. Readers who are interested in this topic are instead encouraged to see [17] and Sect. IV in order to get deeper insights about the problem of the extended multi-target tracking for X-band marine radar data.

A. State Model

The extended target kinematics (position and velocity) are defined in 2D Cartesian coordinates and modeled by the vector $\mathbf{x}_k \triangleq [x_k, \dot{x}_k, y_k, \dot{y}_k]^T$, where x_k, y_k and $\dot{x}_k$, $\dot{y}_k$ are the position and velocity components along the X, Y directions, respectively, and $[\cdot]^T$ is the transpose operator. The extended target's extent (shape and size) is assumed elliptic and is modeled by the positive definite matrix $\mathbf{X}_k$.

Let $\mathbf{Z}^k = \{\mathbf{Z}_m\}_{m=0}^k$ denote all the measurement sets up to and including frame k. The extended target state, i.e. $\mathbf{x}_k$ and $\mathbf{X}_k$, is Gaussian inverse Wishart distributed,

$$p(\mathbf{x}_k, \mathbf{X}_k \mid \mathbf{Z}^k) = \mathcal{N}(\mathbf{x}_k; \hat{\mathbf{x}}_{k|k}, \mathbf{P}_{k|k}) \mathcal{IW}(\mathbf{X}_k; \alpha_{k|k}, \hat{\mathbf{X}}_{k|k}) \quad (1)$$

where $\hat{\mathbf{x}}_{k|k}$ and $\mathbf{P}_{k|k}$ are the expected value and covariance of the Gaussian distribution, and $\hat{\mathbf{X}}_{k|k}$ and $\alpha_{k|k}$ are the expected value and degrees of freedom of the inverse Wishart distribution.

B. Dynamic Model

The target's motion is described by a nearly constant velocity model [3]. The state-update equation is as follows

$$\mathbf{x}_k = \mathbf{F}\mathbf{x}_{k-1} + \mathbf{\Gamma}\mathbf{w}_k \quad (2)$$

where $\mathbf{F} = \tilde{\mathbf{F}} \otimes \mathbf{I}_d$, $\mathbf{I}_d$ is the identity matrix with dimension $d \times d$ (i.e. 2×2 in our case), $\otimes$ denotes the Kronecker product,

$$\tilde{\mathbf{F}} = \begin{bmatrix} 1 & T_s \\ 0 & 1 \end{bmatrix}, \quad (3)$$

T_s is the sampling time, $\mathbf{\Gamma} = \tilde{\mathbf{\Gamma}} \otimes \mathbf{I}_d$,

$$\tilde{\mathbf{\Gamma}} = \sigma_{pos} \cdot \begin{bmatrix} T_s^2/2 \\ T_s \end{bmatrix}, \quad (4)$$

and σ_{pos} represents the process noise (equal in both X and Y directions). The process noise $\mathbf{w}_k$ takes into account the target acceleration and the unmodeled dynamics and it is assumed to be Gaussian with zero-mean and identity covariance matrix.

The time evolution of the extent $\mathbf{X}_k$ is modeled as approximately constant over time. This model is accurate for targets that can be assumed to move linearly, i.e. targets that do not turn significantly (a turn causes the extension to rotate). For the scenarios considered in this paper this assumption is true. Motion models for turning targets can be found in related literature, see e.g. [21].

C. Measurement Model Using Converted Measurements

Measurements of the target's positions are usually provided in polar coordinates (i.e. in range and azimuth) for data acquired by radar systems. However, the target motion is typically modeled in Cartesian coordinates. Hence, a conventional linear Kalman filter can be exploited only after the measurements have been converted from polar to Cartesian coordinates. It is important for the tracking results that the effects of this conversion are properly taken into consideration.

The components of the jth measurement vector at frame k are defined as $\zeta_k^j \triangleq [r_k^j, \theta_k^j]^T$, where r_k^j and θ_k^j are the jth range and azimuth radar measurements at frame k, respectively. These measurements are modeled as the true range and azimuth values, plus measurement errors that are zero-mean Gaussian distributed with standard deviations equal to σ_r and σ_θ, respectively. To convert measurements from polar to Cartesian coordinates we employ the standard coordinate conversion,

$$\mathbf{z}_k^{L,j} \triangleq [x_k^{L,j}, y_k^{L,j}]^T = [r_k^j \cos\theta_k^j, r_k^j \sin\theta_k^j]^T \tag{5}$$

where the superscript L stands for linearization.

Taking the first order terms of the Taylor series expansion of the standard coordinate conversion, i.e. using linearization, we obtain the Cartesian coordinate errors, which have zero-mean and covariance matrix [3]

$$\mathbf{R}^L(\zeta_k^j) = \mathbf{J}(\zeta_k^j)\mathrm{diag}([\sigma_r^2, \sigma_\theta^2])\mathbf{J}^T(\zeta_k^j), \tag{6}$$

where

$$\mathbf{J}(\zeta_k^j) = \begin{bmatrix} \cos\theta_k^j & -r_k^j \sin\theta_k^j \\ \sin\theta_k^j & r_k^j \cos\theta_k^j \end{bmatrix} \tag{7}$$

is the Jacobian matrix, and diag(·) indicates a diagonal matrix.

A remark is related to the validity of the standard coordinate conversion. A rule of thumb is provided in [3]. When it is not valid, the unbiased conversion [3] can be exploited to deal with the problem of converting measurements from polar to Cartesian coordinates. In this case, we have that for the jth measurement at frame k, $\mathbf{z}_k^{U,j} \triangleq [x_k^{U,j}, y_k^{U,j}]^T$, where

$$x_k^{U,j} = x_k^{L,j} b^{-1}, \tag{8}$$

$$y_k^{U,j} = y_k^{L,j} b^{-1}, \tag{9}$$

and $b = \exp(-\sigma_\theta^2/2)$ assuming that the noise in the polar domain is Gaussian distributed.

The covariance matrix is as follows:

$$\mathbf{R}^U(\zeta_k^j) = \begin{bmatrix} \mathbf{R}_{11}^U(\zeta_k^j) & \mathbf{R}_{12}^U(\zeta_k^j) \\ \mathbf{R}_{21}^U(\zeta_k^j) & \mathbf{R}_{22}^U(\zeta_k^j) \end{bmatrix}, \tag{10}$$

where its elements are defined as [3]

$$\begin{aligned} \mathbf{R}_{11}^U(\zeta_k^j) &= (b^{-2} - 2)(r_k^j)^2 \cos^2\theta_k^j \\ &\quad + [(r_k^j)^2 + \sigma_r^2][1 + b^4 \cos 2\theta_k^j]/2, \end{aligned} \tag{11}$$

$$\begin{aligned} \mathbf{R}_{22}^U(\zeta_k^j) &= (b^{-2} - 2)(r_k^j)^2 \sin^2\theta_k^j \\ &\quad + [(r_k^j)^2 + \sigma_r^2][1 - b^4 \cos 2\theta_k^j]/2, \end{aligned} \tag{12}$$

$$\begin{aligned} \mathbf{R}_{21}^U(\zeta_k^j) = \mathbf{R}_{12}^U(\zeta_k^j) &= b^{-2}(r_k^j)^2/2 \sin 2\theta_k^j \\ &\quad + [(r_k^j)^2 + \sigma_r^2]b^4/2 \sin 2\theta_k^j - (r_k^j)^2 \sin 2\theta_k^j. \end{aligned} \tag{13}$$

For the radar data used in this paper the standard coordinate conversion was empirically found to be sufficient, see Sect. V for further details.

We assume, as done in [12], [25], that at each frame there is a set of n_k independent Cartesian position measurements, denoted $\mathbf{Z}_k = \{\mathbf{z}_k^j\}$ (i.e. either $\mathbf{z}_k^{L,j}$ or $\mathbf{z}_k^{U,j}$). The detection set likelihood is

$$p(\mathbf{Z}_k \mid n_k, \mathbf{x}_k, \mathbf{X}_k) = \prod_{j=1}^{n_k} p(\mathbf{z}_k^j \mid \mathbf{x}_k, \mathbf{X}_k). \tag{14}$$

Each detection $\mathbf{z}_k^j$ is modeled as a noisy measurement of a reflection point $\mathbf{y}_k^j$ located somewhere on the extended target. Further, each reflection point is modeled as a point randomly sampled from the target's extension. The detection likelihood is thus

$$p(\mathbf{z}_k^j \mid \mathbf{x}_k, \mathbf{X}_k) = \int p(\mathbf{z}_k^j \mid \mathbf{y}_k^j, \mathbf{x}_k, \mathbf{X}_k) p(\mathbf{y}_k^j \mid \mathbf{x}_k, \mathbf{X}_k) d\mathbf{y}_k^j \tag{15}$$

In other words, the detection likelihood (15) is the marginalization of the reflection point $\mathbf{y}$ out of the estimation problem.

For the type of radar systems considered here the measurement noise is accurately modeled as zero mean Gaussian,

$$p(\mathbf{z}_k^j \mid \mathbf{y}_k^j, \mathbf{x}_k, \mathbf{X}_k) = \mathcal{N}(\mathbf{z}_k^j; \mathbf{y}_k^j, \mathbf{R}(\mathbf{y}_k^j)), \tag{16}$$

where $\mathbf{R}(\mathbf{y})$ is the covariance matrix (i.e. either $\mathbf{R}^L(\mathbf{y})$ using (6) or $\mathbf{R}^U(\mathbf{y})$ using (10)) obtained when converting polar radar detections to Cartesian coordinates. Further,

the reflection points are accurately modeled as uniform samples from the target shape,

$$p(\mathbf{y}_k^j \mid \mathbf{x}_k, \mathbf{X}_k) = \mathcal{U}(\mathbf{y}_k^j; \mathbf{x}_k, \mathbf{X}_k). \tag{17}$$

As suggested by Feldmann et al. [12], for an elliptically shaped target the uniform distribution (17) is approximated by the following Gaussian distribution

$$p(\mathbf{y}_k^j \mid \mathbf{x}_k, \mathbf{X}_k) = \mathcal{N}(\mathbf{y}_k^j; \mathbf{H}\mathbf{x}_k, \rho\mathbf{X}_k) \tag{18}$$

where ρ is a scaling factor. Here $\mathbf{H}$ is a measurement model that selects the position components in the state vector (i.e. $\mathbf{H} = [\mathbf{I}_d, \mathbf{0}_d]$ where $\mathbf{0}_d$ indicates the null matrix with $d = 2$ in our case). In a simulation study Feldmann et al. showed that $\rho = 1/4$ is a good parameter setting. In the result section we will address what is an appropriate parameter setting when using real radar data.

By combining equations (15), (16) and (18), the likelihood is

$$p(\mathbf{z}_k^j \mid \mathbf{x}_k, \mathbf{X}_k) = \int \mathcal{N}(\mathbf{z}_k^j; \mathbf{y}_k^j, \mathbf{R}(\mathbf{y}_k^j)) \mathcal{N}(\mathbf{y}_k^j; \mathbf{H}\mathbf{x}_k, \rho\mathbf{X}_k) d\mathbf{y}_k^j. \tag{19}$$

The marginalization (19) is analytically intractable. To achieve a computationally efficient measurement update, two assumptions are made. First, assume that in (16) the measurement noise covariance can be approximated as $\mathbf{R}(\mathbf{y}_k^j) \approx \mathbf{R}(\mathbf{H}\mathbf{x}_k)$, i.e.

$$p(\mathbf{z}_k^j \mid \mathbf{y}_k^j, \mathbf{x}_k, \mathbf{X}_k) \approx \mathcal{N}(\mathbf{z}_k^j; \mathbf{y}_k^j, \mathbf{R}(\mathbf{H}\mathbf{x}_k)). \tag{20}$$

REMARK In general, this approximation is less accurate the larger the distance is between the reflection point $\mathbf{y}$ and the target's position, as given by $\mathbf{H}\mathbf{x}_k$. This implies that the approximation is less accurate the larger the target is, since a large target means that the distance between the reflection point and position may be large. For the radar sensors and the targets that are considered in this paper, we have empirically found that the approximation is sufficiently accurate.

Following the assumption in (20), applying it in (15), considering (18), and exploiting the product formula for two multivariate Gaussian distributions, we have that

$$p(\mathbf{z}_k^j \mid \mathbf{x}_k, \mathbf{X}_k) \approx \mathcal{N}(\mathbf{z}_k^j; \mathbf{H}\mathbf{x}_k, \rho\mathbf{X}_k + \mathbf{R}(\mathbf{H}\mathbf{x}_k)). \tag{21}$$

Considering that the prior target distribution is Gaussian inverse Wishart, i.e.

$$p(\mathbf{x}_k, \mathbf{X}_k \mid \mathbf{Z}^{k-1}) = \mathcal{N}(\mathbf{x}_k; \hat{\mathbf{x}}_{k|k-1}, \mathbf{P}_{k|k-1}) \times \mathcal{IW}(\mathbf{X}_k; \alpha_{k|k-1}, \hat{\mathbf{X}}_{k|k-1}), \tag{22}$$

we assume that the following approximation holds, i.e.

$$p(\mathbf{z}_k^j \mid \mathbf{x}_k, \mathbf{X}_k) \approx \mathcal{N}(\mathbf{z}_k^j; \mathbf{H}\mathbf{x}_k, \rho\mathbf{X}_k + \mathbf{R}(\mathbf{H}\hat{\mathbf{x}}_{k|k-1})), \tag{23}$$

namely the measurement noise covariance can be approximated by replacing $\mathbf{x}_k$ with its predicted expected value $\hat{\mathbf{x}}_{k|k-1}$.

REMARK This approximation is trivially satisfied when $\mathbf{R}(\cdot)$ is a constant matrix. In general the assumption holds approximately when $\mathbf{R}(\cdot)$ does not vary too much in the uncertainty region for the extended target. Empirically we have found that, for the sensors and targets considered here, the signal to noise ratio is high enough to make the uncertainty region small enough.

Under the two assumptions above, the detection likelihood $p(\mathbf{z}_k^j \mid \mathbf{x}_k, \mathbf{X}_k)$ assumes the same form as in [12] replacing the covariance noise matrix $\mathbf{R}$ with its state-dependent version $\mathbf{R}(\mathbf{H}\hat{\mathbf{x}}_{k|k-1})$. Thus, the measurement update results analogous to the measurement update proposed in [12] by substituting $\mathbf{R}$ with $\mathbf{R}(\mathbf{H}\hat{\mathbf{x}}_{k|k-1})$. This approach is here called *converted measurement extended target tracking* (CM-ETT) and its time and measurement updates are presented in the next section.

III. CONVERTED MEASUREMENTS EXTENDED TARGET FILTERING

In this section we show the time update and measurement update for the models presented in the previous section.

A. Time Update

With the assumed independence between the estimates for centroid kinematics and extension and further assuming independent dynamic models for both of them, the standard Kalman filter prediction equations can be exploited [3], [12]:

$$\hat{\mathbf{x}}_{k|k-1} = \mathbf{F}\hat{\mathbf{x}}_{k-1|k-1}, \tag{24}$$

$$\mathbf{P}_{k|k-1} = \mathbf{F}\mathbf{P}_{k-1|k-1}\mathbf{F}^T + \mathbf{\Gamma}. \tag{25}$$

The prediction of the target's extension comes directly from the hypothesis that the extension does not tend to change over time, i.e.

$$\hat{\mathbf{X}}_{k|k-1} = \hat{\mathbf{X}}_{k-1|k-1}. \tag{26}$$

Finally, the prediction of the degrees of freedom parameter $\alpha_{k|k-1}$ is given as [12]

$$\alpha_{k|k-1} = 2 + \exp(-T_s/\tau)(\alpha_{k-1|k-1} - 2), \tag{27}$$

where τ is a time constant related to the agility with which the target may change its extension over time.

B. Measurement Update

The measurement updated expected value and covariance of the state vector estimate are obtained by a Kalman filter update [12]

$$\hat{\mathbf{x}}_{k|k} = \hat{\mathbf{x}}_{k|k-1} + \mathbf{K}_{k|k-1}(\bar{\mathbf{z}}_k - \mathbf{H}\hat{\mathbf{x}}_{k|k-1}), \tag{28}$$

$$\mathbf{P}_{k|k} = \mathbf{P}_{k|k-1} - \mathbf{K}_{k|k-1}\mathbf{S}_{k|k-1}\mathbf{K}_{k|k-1}^T, \tag{29}$$

where

$$\mathbf{S}_{k|k-1} = \mathbf{H}\mathbf{P}_{k|k-1}\mathbf{H}^T + \frac{\mathbf{Z}_{k|k-1}}{n_k}, \tag{30}$$

$$\mathbf{K}_{k|k-1} = \mathbf{P}_{k|k-1}\mathbf{H}^T\mathbf{S}_{k|k-1}^{-1} \tag{31}$$

are the innovation covariance and the gain, and

$$\mathbf{Z}_{k|k-1} = \rho\hat{\mathbf{X}}_{k|k-1} + \mathbf{R}_k(\mathbf{H}\hat{\mathbf{x}}_{k|k-1}) \tag{32}$$

indicates the predicted covariance of a single measurement. Note that $\mathbf{R}_k(\mathbf{H}\hat{\mathbf{x}}_{k|k-1})$ depends on the predicted expected value $\hat{\mathbf{x}}_{k|k-1}$ (differently from [12] where it is constant) and the posterior of the kinematic state conditioned on $\mathbf{x}_k$ is again assumed to be close to a normal distribution.

The updated expected value and degrees of freedom of the extension estimate $\hat{\mathbf{X}}_{k|k}$ are obtained as follows [12]

$$\hat{\mathbf{X}}_{k|k} = \frac{\alpha_{k|k-1}\hat{\mathbf{X}}_{k|k-1} + \hat{\mathbf{N}}_{k|k-1} + \hat{\mathbf{Z}}_{k|k-1}}{\alpha_{k|k}}, \tag{33}$$

$$\alpha_{k|k} = \alpha_{k|k-1} + n_k, \tag{34}$$

where

$$\hat{\mathbf{N}}_{k|k-1} = \hat{\mathbf{X}}_{k|k-1}^{1/2}\mathbf{S}_{k|k-1}^{-1/2}\mathbf{N}_{k|k-1}(\mathbf{S}_{k|k-1}^{-1/2})^T(\hat{\mathbf{X}}_{k|k-1}^{1/2})^T, \tag{35}$$

$$\hat{\mathbf{Z}}_{k|k-1} = \hat{\mathbf{X}}_{k|k-1}^{1/2}\mathbf{Z}_{k|k-1}^{-1/2}\bar{\mathbf{Z}}_k(\mathbf{Z}_{k|k-1}^{-1/2})^T(\hat{\mathbf{X}}_{k|k-1}^{1/2})^T, \tag{36}$$

$$\mathbf{N}_{k|k-1} = (\bar{\mathbf{z}}_k - \mathbf{H}\hat{\mathbf{x}}_{k|k-1})(\bar{\mathbf{z}}_k - \mathbf{H}\hat{\mathbf{x}}_{k|k-1})^T, \tag{37}$$

and

$$\bar{\mathbf{z}}_k = \frac{1}{n_k}\sum_{j=1}^{n_k}\mathbf{z}_k^j, \tag{38}$$

$$\bar{\mathbf{Z}}_k = \sum_{j=1}^{n_k}(\mathbf{z}_k^j - \bar{\mathbf{z}}_k)(\mathbf{z}_k^j - \bar{\mathbf{z}}_k)^T \tag{39}$$

are the centroid measurement and the measurement spread. Note that the marginalized prior density of the target extension is assumed to be an inverse Wishart density [25]. This implies that the posterior is again of the same form.

IV. GAMMA GAUSSIAN INVERSE WISHART PROBABILITY HYPOTHESIS DENSITY

A multiple extended target tracker is briefly described in this section. The converted measurements model in Sect. II is integrated in the measurement update exploiting the results in Sect. III to obtain an improvement in the targets' size estimation. The core of the tracker is a probability hypothesis density (PHD) filter which provides for each radar frame the kinematics, the size and the shape, as well as the expected number of detections relevant to each target occurring in the surveillance area. The filter is fed with the measurements provided by the detector described in Sect. V-D.

The extended target state ξ_k can be redefined as

$$\xi_k \triangleq (\gamma_k, \mathbf{x}_k, \mathbf{X}_k), \tag{40}$$

where the random vector $\mathbf{x}_k$ and $\mathbf{X}_k$ represent again the kinematic and extension states and $\gamma_k > 0$ is the measurement rate that describes how many measurements the target, on average, generates per frame. The number of target generated measurements is assumed to be Poisson distributed, and γ_k is in this case the Poisson rate [13], [14].

Conditioned on a history of previous measurement sets, $\mathbf{Z}^k$, ξ_k is modeled as a gamma-Gaussian-inverse Wishart (GGIW) distribution [12], [18],

$$p(\xi_k \mid \mathbf{Z}^k) = p(\gamma_k \mid \mathbf{Z}^k)p(\mathbf{x}_k \mid \mathbf{Z}^k)p(\mathbf{X}_k \mid \mathbf{Z}^k) \tag{41a}$$

$$= \mathcal{G}(\gamma_k; \alpha_{k|k}^g, \beta_{k|k})\mathcal{N}(\mathbf{x}_k; \hat{\mathbf{x}}_{k|k}, \mathbf{P}_{k|k}) \tag{41b}$$

$$\times \mathcal{IW}(\mathbf{X}_k; \alpha_{k|k}, \hat{\mathbf{X}}_{k|k})$$

$$= \mathcal{GGIW}(\xi_k; \zeta_{k|k}), \tag{41c}$$

where $\zeta_{k|k} = \{\alpha_{k|k}^g, \beta_{k|k}, \hat{\mathbf{x}}_{k|k}, \mathbf{P}_{k|k}, \alpha_{k|k}, \hat{\mathbf{X}}_{k|k}\}$ is the set of GGIW density parameters.

The probability hypothesis density (PHD) $D_{k|k}(\cdot)$ is an intensity function whose integral is the expected value of the number of targets, and whose peaks correspond to likely target locations, see [15], [29]. The PHD intensity is typically approximated either using Sequential Monte Carlo methods, see [43], or using distribution mixtures, see [20], [42]. In this case, the PHD intensity $D_{k|k}(\cdot)$ at frame k, given the measurement sets up to and including frame k, is approximated by a mixture of GGIW distributions,

$$D_{k|k}(\xi_k) = \sum_{j=1}^{J_{k|k}} w_{k|k}^{(j)}\mathcal{GGIW}(\xi_k; \zeta_{k|k}^{(j)}), \tag{42}$$

where $J_{k|k}$ is the number of components, $w_{k|k}^{(j)}$ is the weight of the jth component, and $\zeta_{k|k}^{(j)}$ is the density parameter of the jth component. On behalf of brevity, no detail for the GGIW tracker is provided. The interested reader can refer to [17] to get all the information related to the time and measurement update equations and the post-processing step (i.e. mixture reduction, track extraction, and track estimation).

V. EXPERIMENTAL RESULTS

The validity of the proposed approach is here demonstrated by exploiting both simulated and real data. The latter are acquired by an X-band marine radar located in La Spezia, Italy. Further to the aim of validating our approach, as already proposed in [31], we exploit, for tracking assessment, the automatic identification system (AIS) [1] static/kinematic messages.

Fig. 1. The X-band marine radar's field of view (in red).

TABLE I
Marine Radar Specifications

Parameter	Specification
Frequency	9.6 GHz
Bandwidth	Adjustable up to 150 MHz
Range resolution	$\Delta r = 1$ m
Antenna type	Rotating slotted waveguide
Antenna angular resolution	$\Delta\theta = 1^\circ$
Antenna angular aperture elevation	20°
Gain	32 dBi
Azimuth antenna speed	0 (stopped) up to 40 revolutions per minute
Polarization	Linear horizontal
Transmitted power	Adjustable 50 mW–5 W (17–37 dBm)
Pulse repetition frequency	Adjustable 350 Hz–10 KHz

The proposed Bayesian ETT method is compared to two other approaches: one random matrix-based tracking algorithm without a model accounting for the sensors' errors, i.e. with $\mathbf{R}_k = \mathbf{0}$ [25], and another random matrix-based approach that exploits a constant covariance matrix $\mathbf{R}$ [12]. The proposed method (both in the case of the standard and the unbiased conversion) is here named converted measurements-ETT (CM-ETT). For a constant covariance matrix $\mathbf{R}$ three different possibilities are tested. They are calculated using (6) by setting θ_k^j to the azimuth mean value on the surveillance area, and letting r_k^j assume one of three values. This gives three different matrices: $\mathbf{R}_1$ calculated for targets that move close to the sensor around range 0.5 km; $\mathbf{R}_2$ calculated for range 2 km, corresponding to the middle of the considered surveillance area; and $\mathbf{R}_3$ hypothesizes that the target sails in a longer range area, around 4 km range.

This section is organized as follows. A description of the X-band marine radar experiment is provided to the reader in Sect. V-A. The real datasets used for the validation of the approach and the AIS message format are briefly illustrated in Sects. V-B and V-C, respectively. The detection strategy is presented in Sect. V-D, while, Sects. V-E and V-F are related to the analysis of the results on simulated and real data, respectively.

A. X-band Marine Radar Experiment

The X-band marine radar is a coherent linear frequency modulated continuous wave radar [38]. It is a compact and lightweight system, still maintaining a high performance with relatively simple electronics, since the transmitted power is low and constant.

The radar is installed in the Gulf of La Spezia (Italy) (see the radar's field of view in Fig. 1). The use of pulse compression [44] and a small transmitted power make it a compact, quickly deployable, and scalable system, used for research in the areas of extended target detection and tracking, with application to surveillance of small craft at short to medium ranges (maximum 5–6 km) for harbor protection and coastal surveillance.

The marine radar has an antenna mounted on a rotor with variable speed of rotation and the possibility to lock and hold the position towards a specific direction with 0.1° accuracy. The main radar parameters are shown in Tab. I. The radiating system for this node consists of two slotted waveguide antennas, one for transmitting and another for receiving, both using linear horizontal polarization. Nevertheless, cross polar vertical-horizontal signatures can be collected in bistatic mode. The high directivity of the slotted waveguide allows a precise determination of the angular position of a target, also allowing the acquisition of targets at long distance with small power.

B. Datasets

Ten datasets have been acquired by the X-band marine radar located in the Gulf of La Spezia, Italy. They have been used for the performance assessment of our approach. The 10 AIS tracks, one for each dataset, are depicted in Fig. 2. They have been generated by 8 different ships. The main features of these ships are briefly outlined below:

- *Grand Holiday* is a Bahamian passenger (cruise) ship with Maritime Mobile Service Identity (MMSI) equal to 255803790. The size of this ship is 222 m × 32 m. The gross tonnage is 46052 t.
- *Palinuro* is a three-masted, iron-hulled barquentine, active as a sails training vessel for the Italian Navy. The MMSI is equal to 247939000. The size of this ship is 59 m × 10 m.
- *Fabio Duo* is an Italian cargo with MMSI equal to 247241500. The size of this ship is 80 m × 16 m. The gross tonnage is 2080 t.
- *Euro* is an Italian passenger ship with MMSI equal to 247030500. The size of this ship is 28 m × 6 m.
- *Monokini* is a pleasure craft with MMSI equal to 6904672. The size of this ship is 45 m × 8 m.

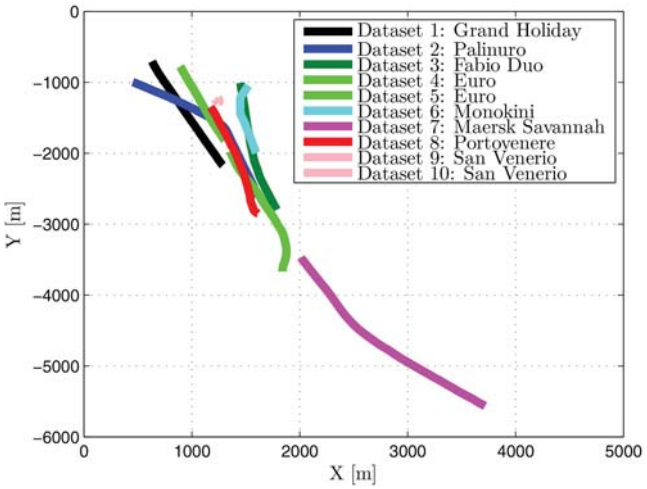

Fig. 2. AIS tracks for all the analyzed datasets.

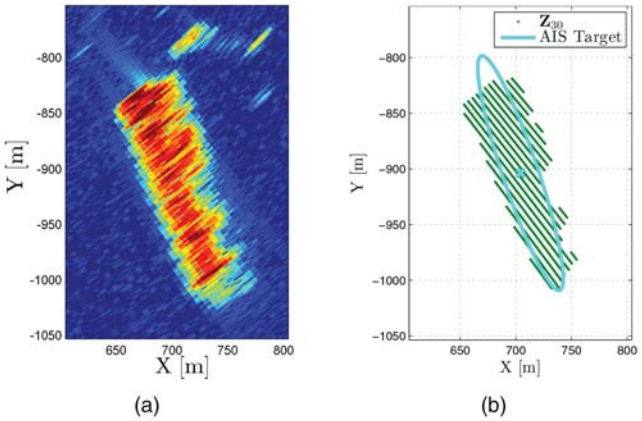

Fig. 3. (a) Amplitude of X-band marine radar data and (b) detections with AIS information for Frame 30 on the *Grand Holiday* dataset.

- *Maersk Savannah* is a Danish container ship with MMSI equal to 219231000. The size of this ship is 334 m × 45 m. The gross tonnage is 92293 t.
- *Portovenere* is an Italian tug with MMSI equal to 247076200. The size of this ship is 28 m × 10 m. The gross tonnage is 279 t.
- *San Venerio* is an Italian tug with MMSI equal to 247841000. The size of this ship is 31 m × 10 m. The gross tonnage is 307 t.

C. AIS Data

Ships and vessels exceeding a given gross tonnage[1] are equipped with AIS transponders for position-reporting, as established by the SOLAS Convention [1]. Ships repeatedly broadcast their name, position, and other details for automatic display on nearby ships. While this allows ships to be aware and keep track of other ships in their immediate vicinity, coastal states will also be able to receive, plot, and log the data by means of base stations along the coast. AIS reports contain both dynamic information (e.g. latitude, longitude, course-over-ground (COG), speed-over-ground (SOG), time) and static information (e.g. vessel type, size information).

To allow their proper use as ground truth for our applications, AIS ship reports are checked in order to remove possible outliers, missing position reports, and unreliable data. An interpolation phase is also required to align in time radar data and AIS contacts.

D. Detection Strategy

Each radar image is processed by a detector to obtain a cloud of detections that represents the input for the Bayesian extended target tracking approaches. In this paper, we exploit a maximum likelihood detector, which represents a good trade-off between computational burden and performance. Generally speaking, other more computationally demanding approaches are possible, i.e. an ordered statistic-based constant false alarm rate (CFAR) detector [36], but their comparison is here considered out of scope.

Two assumptions are made in this phase. First, the conditional independence among nearby pixels is assumed. Furthermore, the distributions of the power images under the *target* and *non-target* hypotheses are considered exponential. The rate parameters $\lambda_t > 0$ (i.e. under *target* hypothesis) and $\lambda_{nt} > 0$ (i.e. under *non-target* hypothesis), which characterize the whole exponential distributions, are estimated using the *k-means* clustering algorithm [23]. An example of detections for Frame 30 on the *Grand Holiday* dataset is depicted in Fig. 3.

E. Simulated Results

The analysis of results reached by the compared algorithms on simulated data is here performed. Three kinds of simulations are exploited in order to understand the capabilities of the approach to work in similar conditions with those expected in the real-world. First, a ship of 80 m × 30 m has been simulated sailing on a straight line from 1 km to 4 km along the range direction using a nearly constant velocity model [3] with zero-mean Gaussian noise described by the parameter σ_{pos}, see Eq. (2). The spread of the detections is Gaussian distributed in polar coordinates according to the used model with scaling parameter ρ equal to 1. The simulator parameters are shown in Tab. II.

Fig. 4 shows the comparison between the standard, see Eq. (5), and the unbiased, see Eqs. (8) and (9), conversions. We can easily see that the outcomes provided by both the models are equivalent (for both kinematic and size estimations). This further corroborates the validation limit rule of thumb in [3], which claims the equivalence between the two models for the considered radar and surveillance area extension. Indeed, following

[1]The AIS is required for all the ships exceeding 300 gross tonnage and engaged on international voyages, for all cargo ships of 500 gross tonnage, not engaged on international voyages, and all passenger ships. On average, a gross weight of 300 t corresponds to a length of about 25 m.

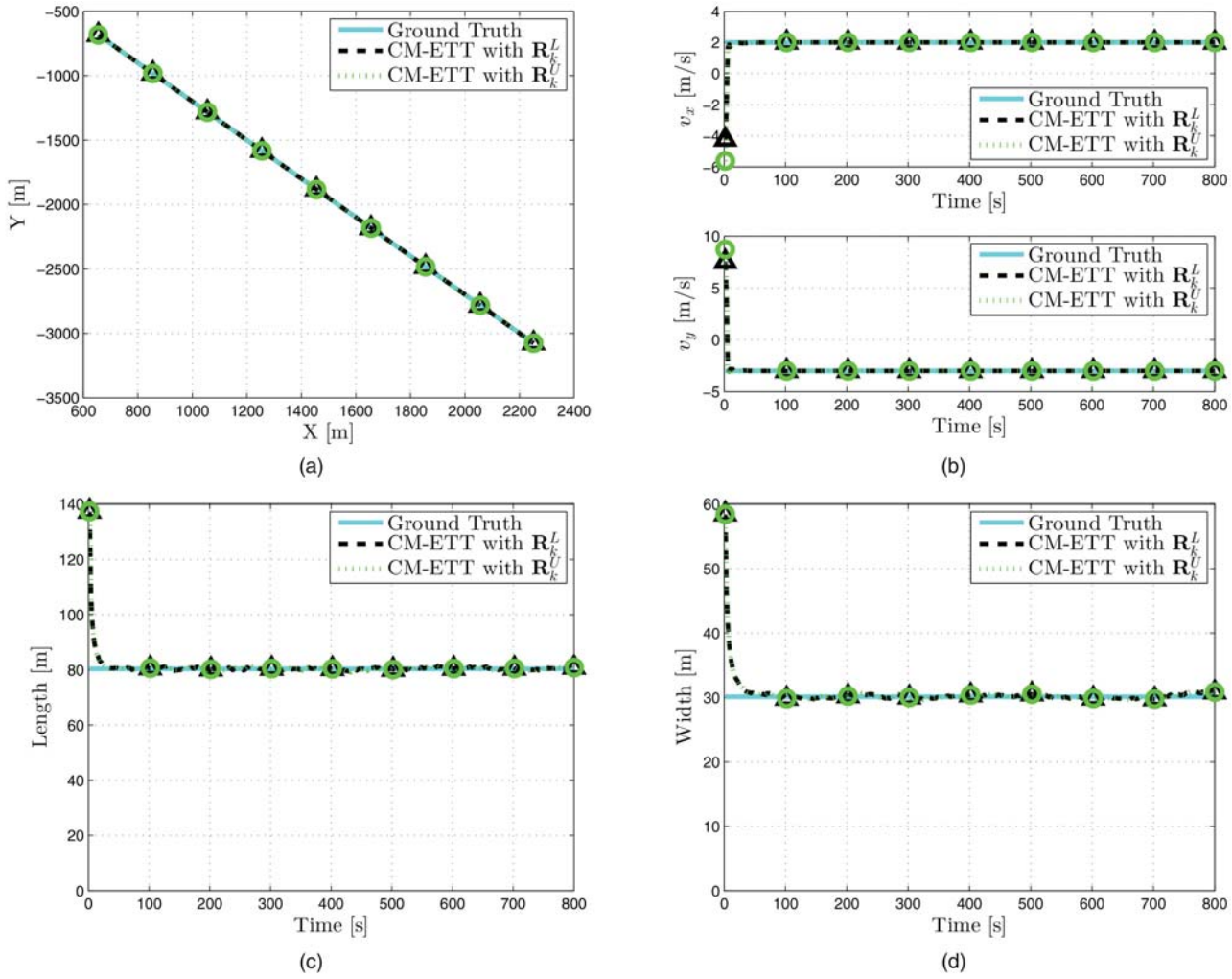

Fig. 4. (a) Position, (b) velocity, (c) length, and (d) width estimations for the proposed CM-ETT approaches on simulated data. Triangular markers are used for indicating the approach using the standard coordinate conversion model, while, circles are exploited for the unbiased conversion.

TABLE II
Parameter Setting Simulator

Parameter	Value	Specification
T_s	2 s	Sampling time
σ_{pos}	10^{-4}ms^{-2}	Std. process noise
Σ	$\begin{bmatrix} 0.6653 & -0.6453 \\ -0.6453 & 1.1764 \end{bmatrix} \cdot 10^3$	Cov. spread target
$k_{\max}$	400	Number of frames
N_d	2000	Num. detects. frame
σ_r^s	0.5 m	Std. noise range
σ_θ^s	0.5°	Std. noise azimuth

the above-mentioned rule, the maximum range $r_{\max}$ that allows proper use of the standard coordinate conversion is defined as

$$r_{\max} = 0.4\frac{\sigma_r}{\sigma_\theta^2}; \tag{43}$$

that is, by substituting the values in Tab. IV, about 3 km, in agreement with the defined surveillance area. Thus, in order to ease the reading of the following results, from hereon we will omit the unbiased conversion.

REMARK The rule of thumb in (43) results satisfied in the most of radar systems, but this is not the case in sonar systems or in long range radar with small σ_r and relatively large σ_θ. When the above-mentioned condition is not verified, the unbiasedness property is not valid and the unbiased conversion has to be exploited instead of the simpler linearization.

The estimations provided by the compared approaches are depicted in Fig. 5. The outcomes confirm the ability of the proposed models to properly take into account the measurement noise. Because the analyzed case shows a ship that sails radially with respect to the radar position and the inaccuracy in range is less than the one in azimuth (as we will see after for the first real case), no difference is perceptible along the range direction (i.e. the target's length). The advantages are instead obvious along the azimuth direction (i.e. the target's width). More specifically, comparing the proposed approach with the one using $\mathbf{R}_k = \mathbf{0}$ or the one

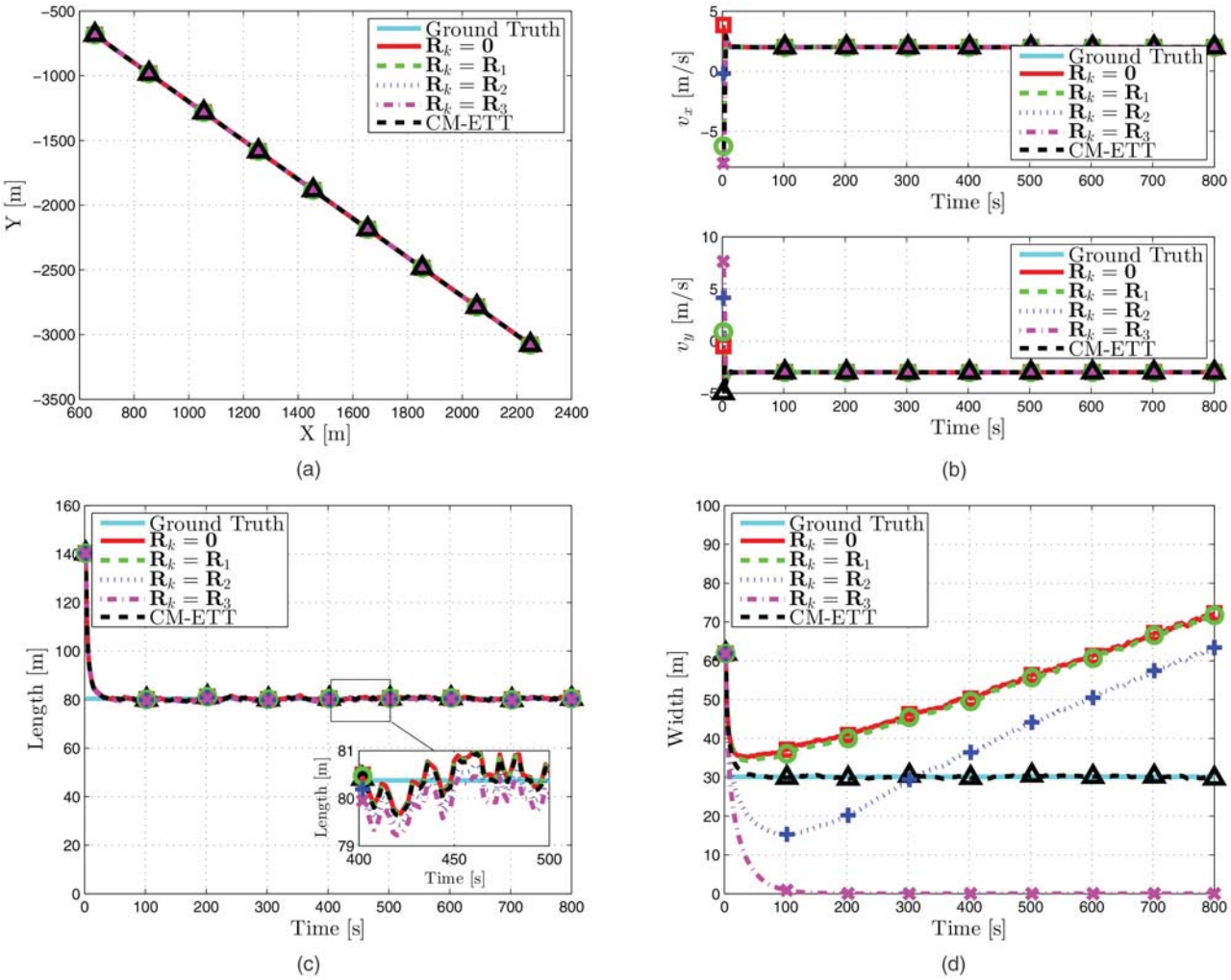

Fig. 5. (a) Position, (b) velocity, (c) length, and (d) width estimations for the compared approaches on simulated data for a target that follows a radial track.

using $\mathbf{R}_1$ it is clear that the more the target obtains large values of range, the greater the advantages are (see the differences for high time values). Both $\mathbf{R}_k = \mathbf{0}$ and $\mathbf{R}_1$ result in the width being overestimated. Using $\mathbf{R}_3$ gives the opposite behavior, i.e. the width is underestimated. Finally, $\mathbf{R}_2$ gives a performance that is in-between the results of the $\mathbf{R}_1$ and the $\mathbf{R}_3$ algorithms.

The second test case simulates the target sailing in an almost constant range track. Because we simulate an almost constant range track the opposite width/length estimation results are expected with respect to the previous test case. Fig. 6 shows the kinematic and size estimations provided by the compared approaches. Again, the CM-ETT shows its ability to properly estimate both the length and width parameters. As expected, considerable advantages are shown for the cross-range size estimation (length), while comparable performance can be pointed out for the estimation of the width parameter (along-range size).

The third test case in Fig. 7, where a non-along constant range and non-radial track is simulated, corroborates that the proposed CM-ETT gives improved performance both for the cross-range size and the along-range size. Again, comparing the proposed approach with the one using $\mathbf{R}_k = \mathbf{0}$ or the one using $\mathbf{R}_1$ it is clear that the more the target obtains large values of range, the greater the advantages are. Finally, $\mathbf{R}_2$ represents again a good compromise among the compared approaches.

A final note is related to the estimation of the kinematic parameters (i.e. position and velocity). All the algorithms perform well and the results reached by them can be considered comparable, see Figs. 5(a)–(b), Figs. 6(a)–(b), and Figs. 7(a)–(b). Indeed, for this application, the sensors' inaccuracies mainly impact the estimation of the ship sizes instead of the kinematic parameters.

Finally, Tab. III shows the performance assessment for all the three simulated test cases. Best results are in boldface. The root mean square errors (RMSEs) in position (i.e. ϵ^{pos}), velocity (i.e. ϵ^{vel}), width (i.e. ϵ^{wid}), and length (i.e. ϵ^{len}) are calculated. Furthermore, the RMS Frobenius error (FE) (i.e. ϵ^{FE}) between the simulated (reference) matrix $\mathbf{S}$, which describes the ellipsoidal simulated target, and the estimations provided by the 5 compared approaches $\hat{\mathbf{X}}$ is shown in Tab. III. This is defined as $\|\hat{\mathbf{X}} - \mathbf{S}\|_F$, where $\|\cdot\|_F$ is the Frobenius

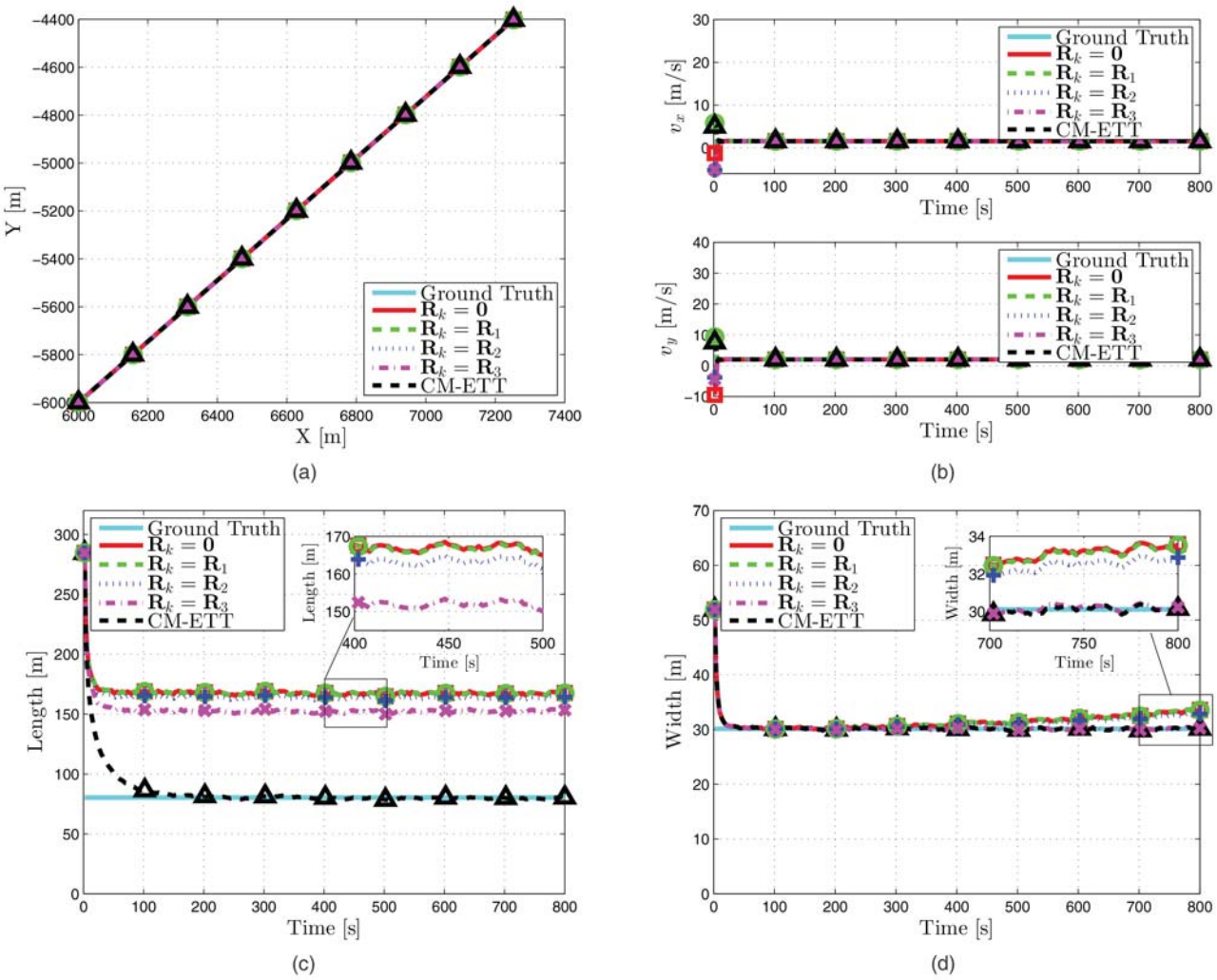

Fig. 6. (a) Position, (b) velocity, (c) length, and (d) width estimations for the compared approaches on simulated data for a target that follows an almost along constant range track.

TABLE III
Performance Assessment on Simulated Data

Test Cases	Methods	ϵ^{pos}	ϵ^{vel}	ϵ^{wid}	ϵ^{len}	ϵ^{FE}
Radial Track	$\mathbf{R}_k = \mathbf{0}$	**0.242**	**0.003**	25.8	**0.4**	595.0
	$\mathbf{R}_k = \mathbf{R}_1$	**0.242**	**0.003**	25.2	**0.4**	578.3
	$\mathbf{R}_k = \mathbf{R}_2$	**0.242**	**0.003**	17.3	0.5	361.5
	$\mathbf{R}_k = \mathbf{R}_3$	0.247	**0.003**	30.1	0.6	249.8
	CM-ETT	**0.242**	**0.003**	**0.2**	**0.4**	**18.9**
Almost Constant Range Track	$\mathbf{R}_k = \mathbf{0}$	0.441	**0.004**	1.6	87.1	5414.6
	$\mathbf{R}_k = \mathbf{R}_1$	0.441	**0.004**	1.6	86.9	5396.0
	$\mathbf{R}_k = \mathbf{R}_2$	0.441	**0.004**	1.3	83.5	5117.4
	$\mathbf{R}_k = \mathbf{R}_3$	0.441	**0.004**	**0.2**	72.1	4232.3
	CM-ETT	**0.439**	**0.004**	**0.2**	**1.4**	**56.8**
Non-along Constant Range/Non-radial Track	$\mathbf{R}_k = \mathbf{0}$	**1.545**	**0.004**	8.1	12.3	677.9
	$\mathbf{R}_k = \mathbf{R}_1$	**1.545**	**0.004**	7.9	12.0	659.8
	$\mathbf{R}_k = \mathbf{R}_2$	1.546	**0.004**	5.1	7.4	401.2
	$\mathbf{R}_k = \mathbf{R}_3$	1.548	**0.004**	29.8	8.1	584.2
	CM-ETT	1.546	**0.004**	**0.2**	**0.4**	**18.2**

norm. This further metric is also able to capture all the differences between estimated and reference matrices, e.g. due to target rotations. The first samples are left out in the calculation of the errors because of the random initializations of the compared approaches. Conclusions as above can be drawn starting from the analysis of the

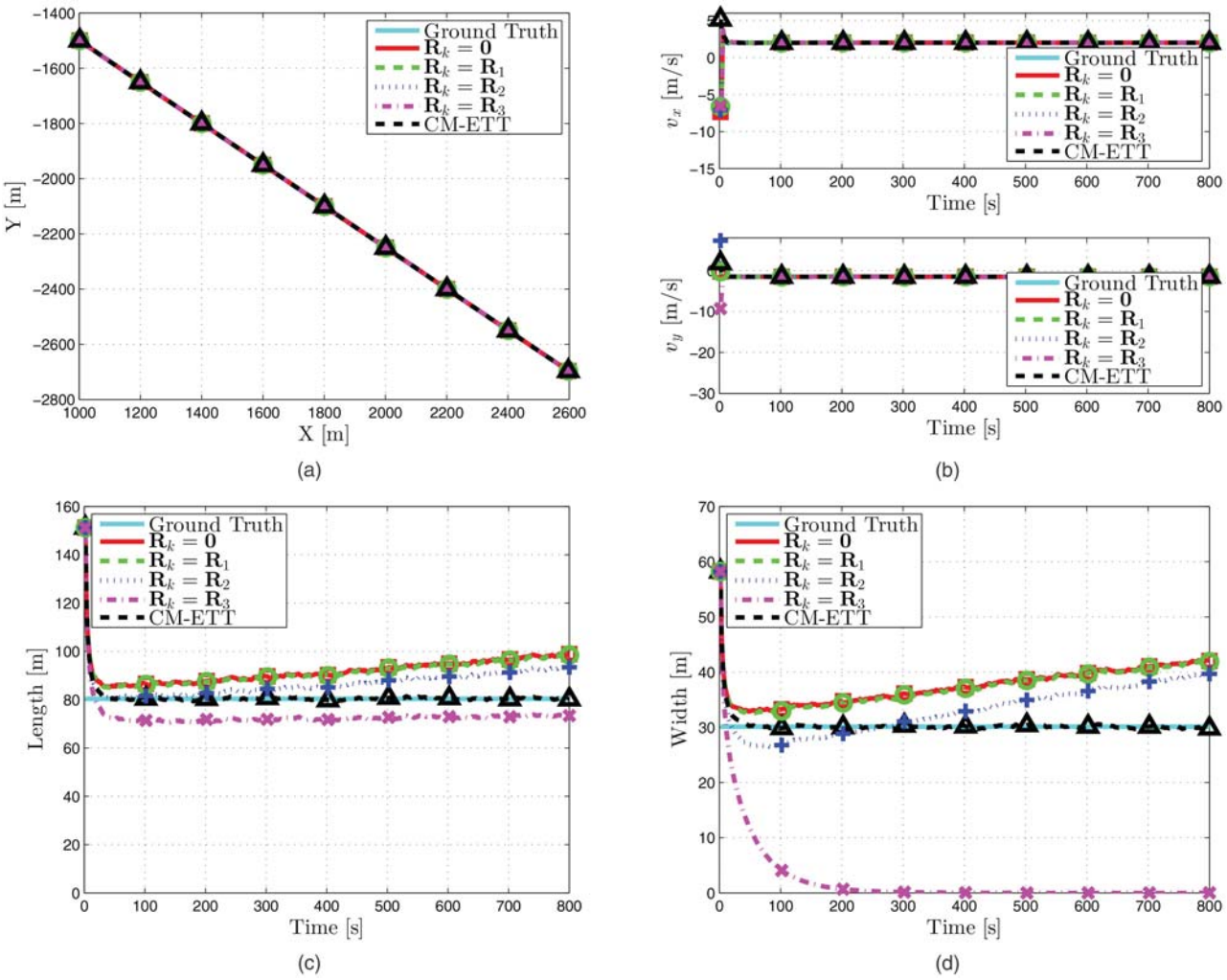

Fig. 7. (a) Position, (b) velocity, (c) length, and (d) width estimations for the compared approaches on simulated data for a target that follows a non-radial and non-along constant range track.

outcomes in the table. These results will be further corroborated by the analysis of the real data provided in the next subsection.

F. Real X-band Marine Radar Data

The description of the outcomes on real data acquired by the X-band marine radar described in Sect. V-A is here provided. The main features of the 8 ships that generate the 10 datasets are shown in Sect. V-B.

Initially, we determine an appropriate value for the parameter ρ (cf. Eq. (18)). Two values of ρ are tested using the CM-ETT approach. In a simulation study presented by Feldmann et al. [12], it is suggested to use $\rho = 1$ to model a Gaussian spread of the detections, while $\rho = 1/4$ models a uniform distribution. Fig. 8 clearly shows that the CM-ETT with $\rho = 1/4$ performs better obtaining a closer match with the AIS ship information. This experimental analysis confirms that data with a uniform detection spread is best modeled by $\rho = 1/4$. In the remainder of the paper, the compared extended target filters are implemented with $\rho = 1/4$. The other tracking parameters used in the experiments are shown in Tab. IV. The sampling time T_s is indicated ranging from 2 s to 5 s. The reason why we have a range instead of a fixed value is that the azimuth antenna speed to acquire the 10 real datasets is different from a dataset to the other, see Tab. I for the radar specifications. Hence, we have different parameters' configuration in order to obtain a trade-off between the sampling time and the number of samples acquired along the azimuth direction, which, for instance, can have an impact on the aliasing. Therefore, the T_s parameter used in the tracking approach can be directly derived by the selected azimuth antenna speed value θ (i.e. $T_s = 60/\theta$). The τ parameter is instead adjusted according to the used T_s value. τ is related to the agility with which the target may change its extension over time. Thus, the datasets with lower T_s values tend to have a more static (i.e. less variable along frames) target extensions (i.e. higher τ parameters are advisable). This is due to the fact that targets sail for a higher number of frames in the same zone and, thus the acquisition system tends to have a same target representation (i.e. less variable target extensions are expected). However, the tuning of

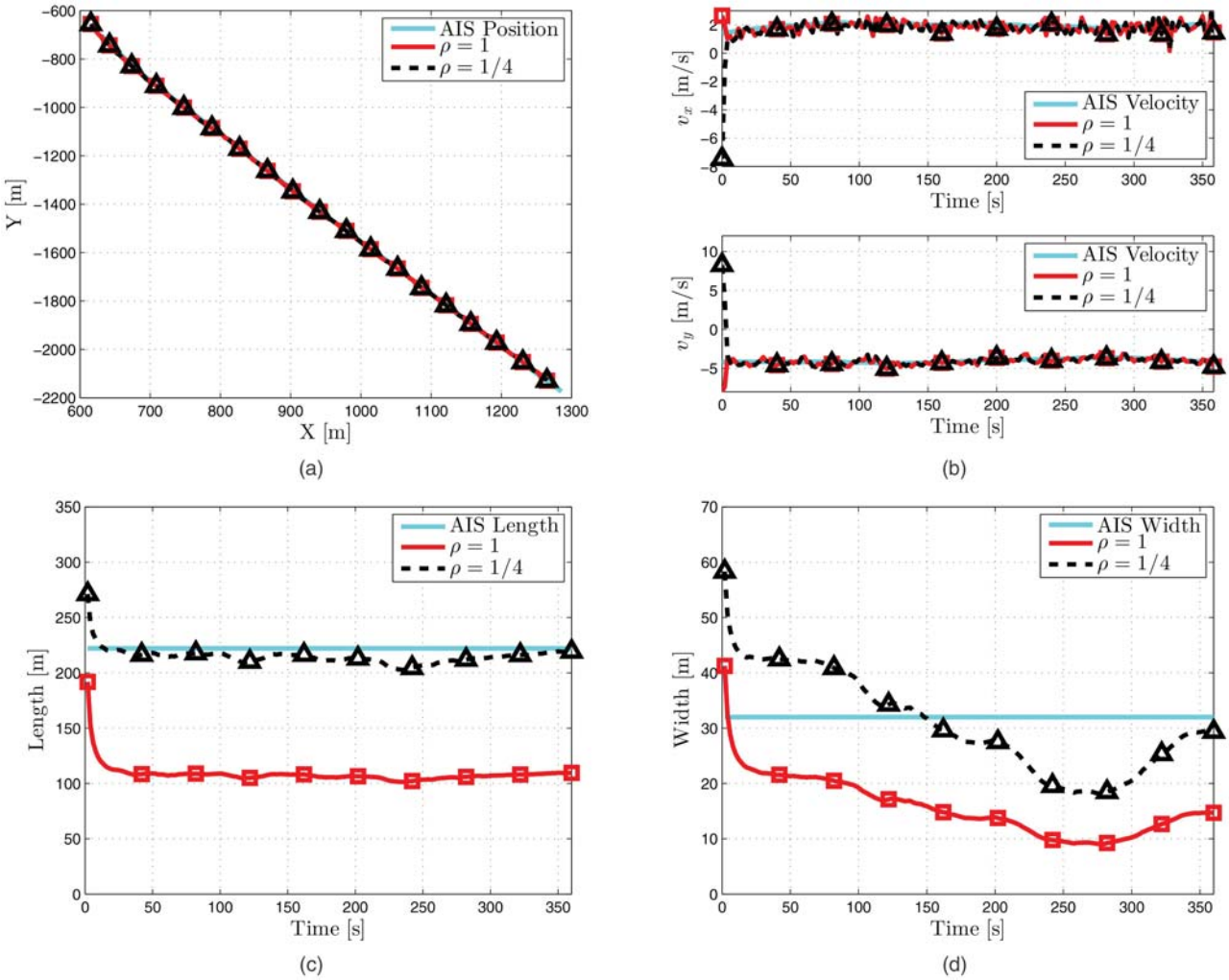

Fig. 8. (a) Position, (b) velocity, (c) length, and (d) width estimation for the CM-ETT using $\rho = 1$ (red solid line) and $\rho = 1/4$ (black dashed line) on the *Grand Holiday* dataset.

TABLE IV
Parameter Setting Real Cases

Parameter	Value	Specification
T_s	2 s–5 s	Sampling time
τ	10/5	Agility object size
σ_{pos}	0.2 ms^{-2}	Std. process noise
$v_{\max}$	10 ms^{-1}	Maximum velocity
σ_r	$\Delta r/2$ (see Tab. I)	Std. noise range
σ_θ	$\Delta\theta/2$ (see Tab. I)	Std. noise azimuth

this parameter as the other parameters in Tab. IV cannot be considered critical, e.g. σ_{pos} and $v_{\max}$ have simply been tuned according to the kinds of targets and the area under test (i.e. medium and large ships that sail in the near coastal area).

A graphic representation of the gains in estimating the size by properly accounting for the measurement noise is provided in Fig. 9 on the *Grand Holiday* dataset. The target, in this case, is moving toward higher range values in an almost radial direction, as can be seen in Fig. 2. Six frames are depicted in Fig. 9 starting from Frame 30 to Frame 180 with temporal resolution equal to 60 s (i.e. an image every 30 frames). We only compare results using the proposed approach and using $\mathbf{R}_k = \mathbf{0}$, because showing all results makes the figures too cluttered. The more the ship sails toward high range values (i.e. the higher the frame number), the greater the spread of the detections. This behavior is mainly due to the polar geometry of the acquisition of the radar.

A first remark is related to Fig. 9(a). Indeed, it is simple to see that in the radar's short range operating region, the proposed model that compensates the radar's noise effects does not gain advantage with respect to the $\mathbf{R}_k = \mathbf{0}$ model. The advantages between the proposed approach and the $\mathbf{R}_k = \mathbf{0}$ model become more evident with increasing range. Note that due to the almost radial track, the target width parameter shows the greatest performance gain. A better match between the algorithm that runs with the proposed model and the ground-truth is straightforward. These outcomes confirm the simulations and they are shown in Figs. 10(c) and (d). Kinematic features are well captured by all the

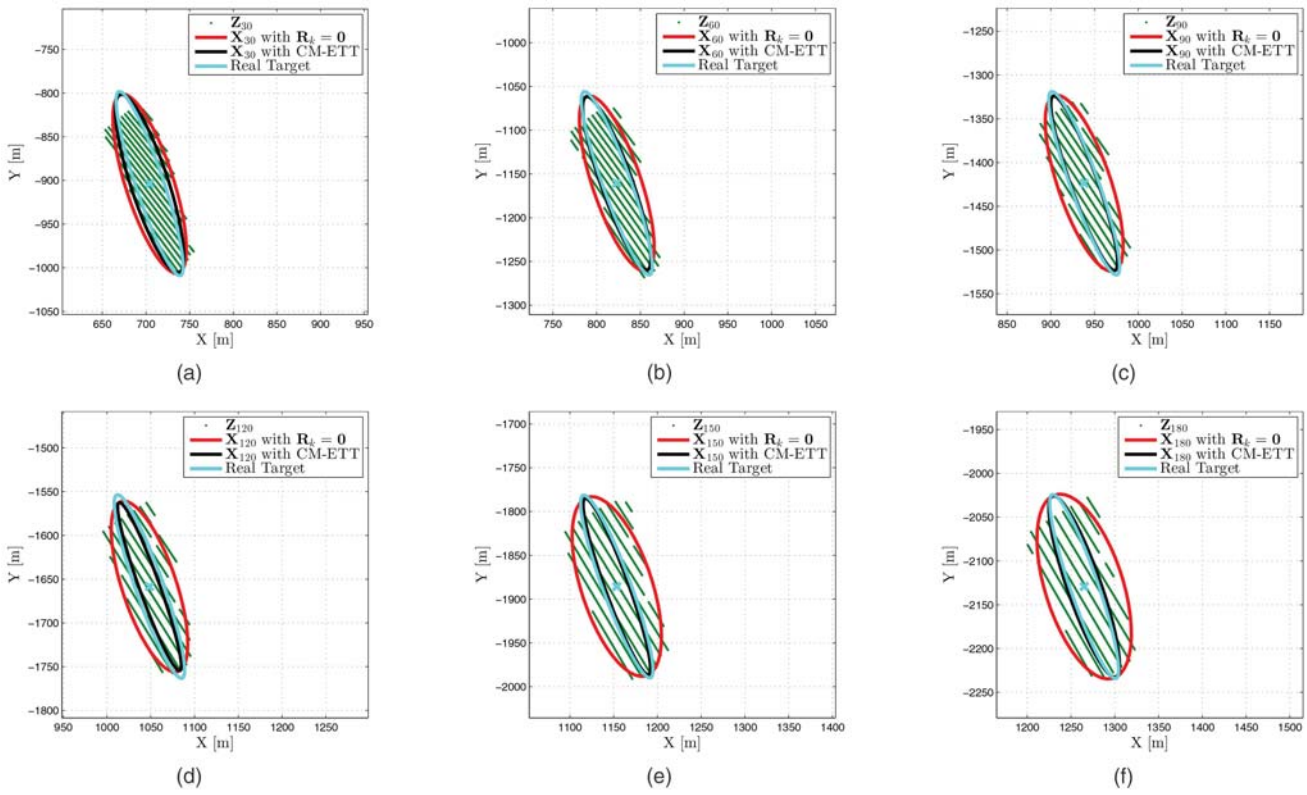

Fig. 9. Estimated ellipsoids provided by the $\mathbf{R}_k = \mathbf{0}$, the CM-ETT, and the ground-truth on the *Grand Holiday* dataset. (a) Frame 30. (b) Frame 60. (c) Frame 90. (d) Frame 120. (e) Frame 150. (f) Frame 180.

TABLE V
Performance Assessment on Real Data

Methods	ϵ^{pos} [m]	ϵ^{vel} [ms^{-1}]	ϵ^{wid} [m]	ϵ^{len} [m]
$\mathbf{R}_k = \mathbf{0}$	**35.4**	0.85	38.4	41.0
$\mathbf{R}_k = \mathbf{R}_1$	**35.4**	0.85	37.5	39.6
$\mathbf{R}_k = \mathbf{R}_2$	**35.4**	0.84	23.5	26.8
$\mathbf{R}_k = \mathbf{R}_3$	**35.4**	**0.80**	18.0	21.6
CM-ETT	**35.4**	0.84	**11.8**	**14.3**

approaches, see Figs. 10(a) and (b). For the error in position, a small displacement between the AIS reports and the estimations provided by the presented algorithms can be pointed out. This is due to the fact that the AIS reports the position of the AIS transponder, while the algorithms estimate the position of the center of the target, which generally speaking, can differ from the AIS transponder's position.

A further test case on the *Portovenere* dataset is also detailed in Fig. 11. This dataset is composed of 130 frames. The AIS track is depicted in Fig. 2. Advantages in the size estimations for the proposed model can be easily pointed out, see Figs. 11(c) and (d). Again, no gain can be seen in the estimation of the kinematic parameters, see Figs. 11(a) and (b). In this case, due to the non-radial track direction, these benefits can be appreciated on both length and width size estimations.

To further corroborate the validity of the proposed approach in providing an improved method of estimating the targets' size and to have a more significant statistical analysis, 8 further real test cases have been performed (the total amount of frames analyzed by the presented algorithms is about 10^3). On behalf of brevity, the results are summarized in Tab. V, where the RMSEs in position ϵ^{pos}, velocity ϵ^{vel}, width ϵ^{wid}, and length ϵ^{len} averaged on all the datasets are shown. The Frobenius error is not available for the real test cases because of the lack of the targets' real orientation in the AIS information. Best results are in boldface. Due to the random initialization of the algorithms, the first frames are neglected to evaluate the RMSEs. No gain can be pointed out for the kinematic parameters' estimation and the outcomes can be considered good in the light of the above-mentioned considerations with regard to the AIS information. The advantages are clear and the errors in both width and length are significantly reduced by properly considering the radar's measurement noise. The RMSEs in width are 11.8 m for the CM-ETT algorithm, 18.0 m for the $\mathbf{R}_3$ method, and 38.4 m in the case of the $\mathbf{R}_k = \mathbf{0}$ approach. Whereas, the RMSEs in length are 14.3 m, 21.6 m, and 41.0 m, respectively. A histogram representation of the absolute errors in width and length for the compared algorithms is depicted in Fig. 12. The results for $\mathbf{R}_1$ and $\mathbf{R}_2$ are worse than the results for $\mathbf{R}_3$, therefore we only compare the proposed CM-ETT filter to $\mathbf{R}_3$ and $\mathbf{R}_k = \mathbf{0}$. Same conclusions as in Tab. V can be drawn.

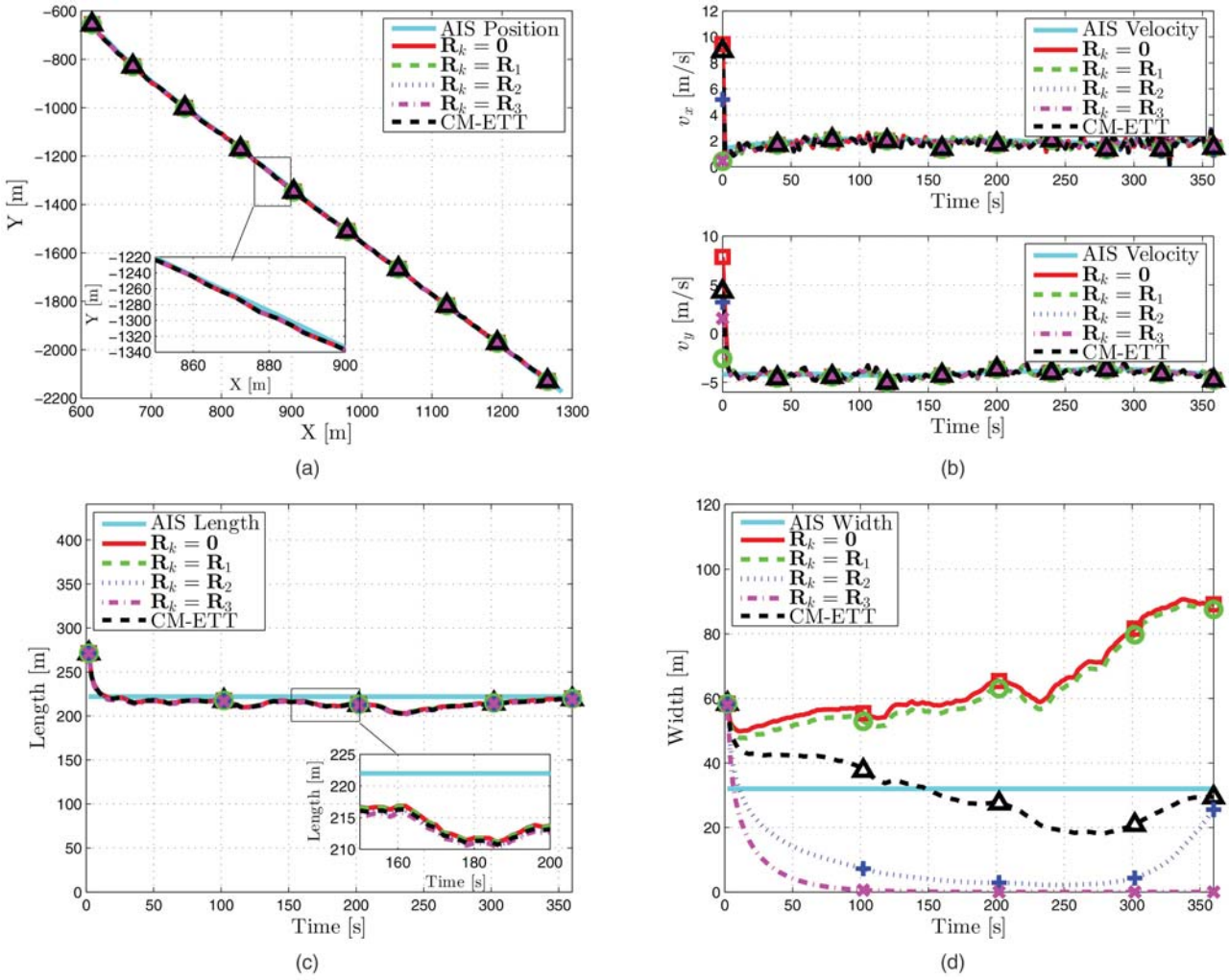

Fig. 10. (a) Position, (b) velocity, (c) length, and (d) width estimations for the compared approaches on the *Grand Holiday* dataset.

It is evident that by properly modeling the polar measurement noise the errors in both width and length are significantly reduced. For the data used here, the average gains of the proposed CM-ETT approach are 70% compared to the $\mathbf{R}_k = \mathbf{0}$ approach and 35% with respect to $\mathbf{R}_3$ for the targets' width estimation accuracy, while advantages of 65% and 34%, respectively, can be observed for the targets' length estimation accuracy.

VI. MULTI-TARGET EXPERIMENTAL RESULTS

In this section the experimental results for the case of multiple extended targets in a cluttered environment are shown. The performance metrics used to assess the quality of the approach are presented first. Afterwards, the experimental results on a real dataset acquired by the X-band marine radar located in the Gulf of La Spezia, Italy, are described.

A. Performance Metrics

This subsection is devoted to the description of the performance metrics, already introduced in [31], suitable for performance assessment in a multiple target and cluttered environment. They are briefly listed, below:

- The **time-on-target** (ToT) is defined as the ratio between the time during which the tracker follows the target and the whole time duration of the true target trajectory. Its ideal value is 1.
- The **false alarm rate** (FAR) is defined as the number of false track contacts normalized with the recording interval and the area of the surveyed region. Its ideal value is 0 that indicates no false alarm.
- The **track fragmentation** (N^{TF}) is calculated by summing the number of radar tracks associated with a unique AIS track. It provides a measurement of the track fragmentation (TF). The ideal value is 1.
- The **tracker accuracy** (TA) is evaluated using the errors in position (ϵ^{pos}), velocity (ϵ^{vel}), length (ϵ^{len}), and width (ϵ^{wid}). Average values along frames are provided as overall indexes. The ideal values are 0.

B. Experimental Results

The assessment is conducted on real data acquired by the X-band marine radar. The main parameters used for the GGIW-PHD approach are summarized in Tab. VI. The dataset consists of 260 frames. AIS data

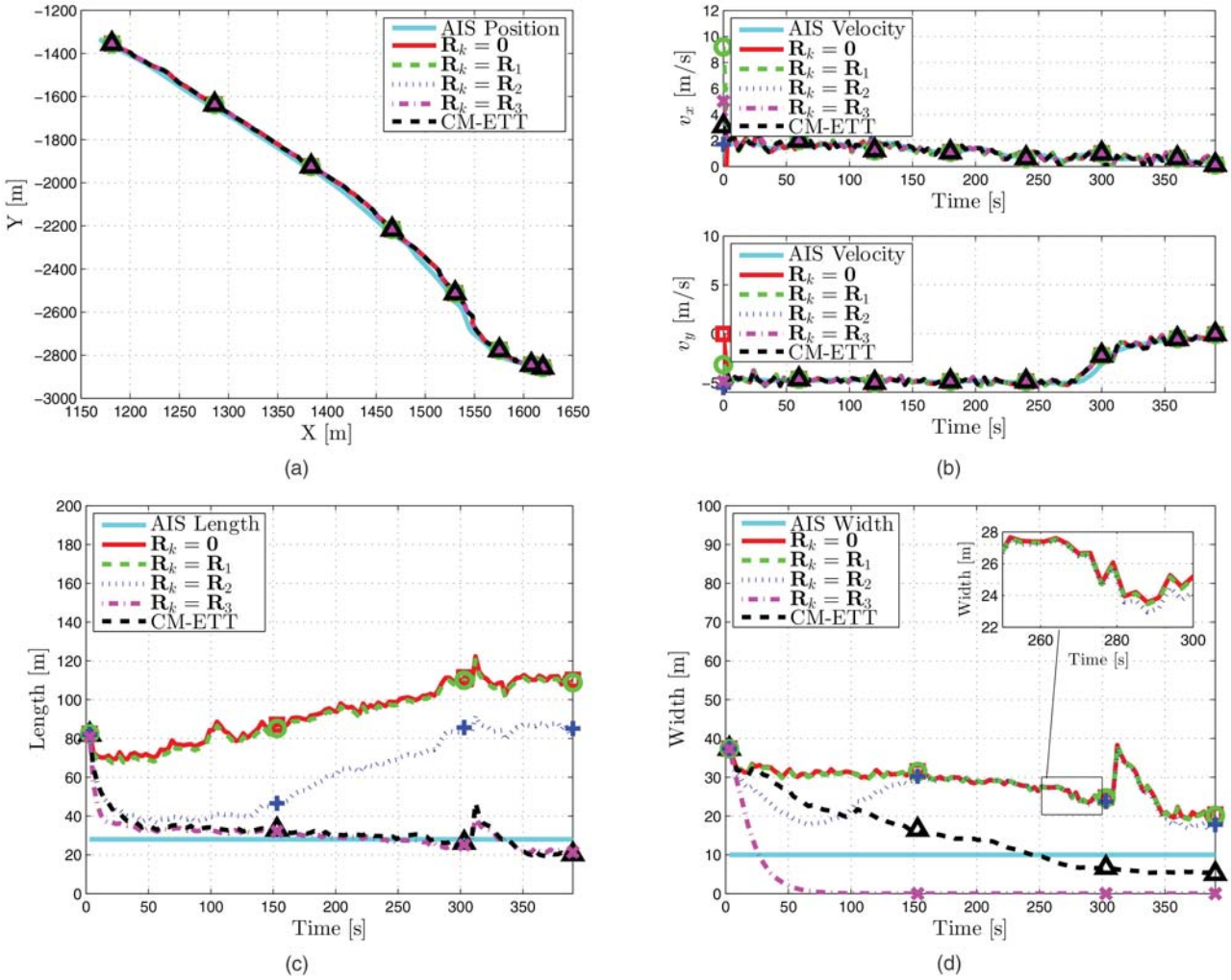

Fig. 11. (a) Position, (b) velocity, (c) length, and (d) width estimations for the compared approaches on the *Portovenere* dataset.

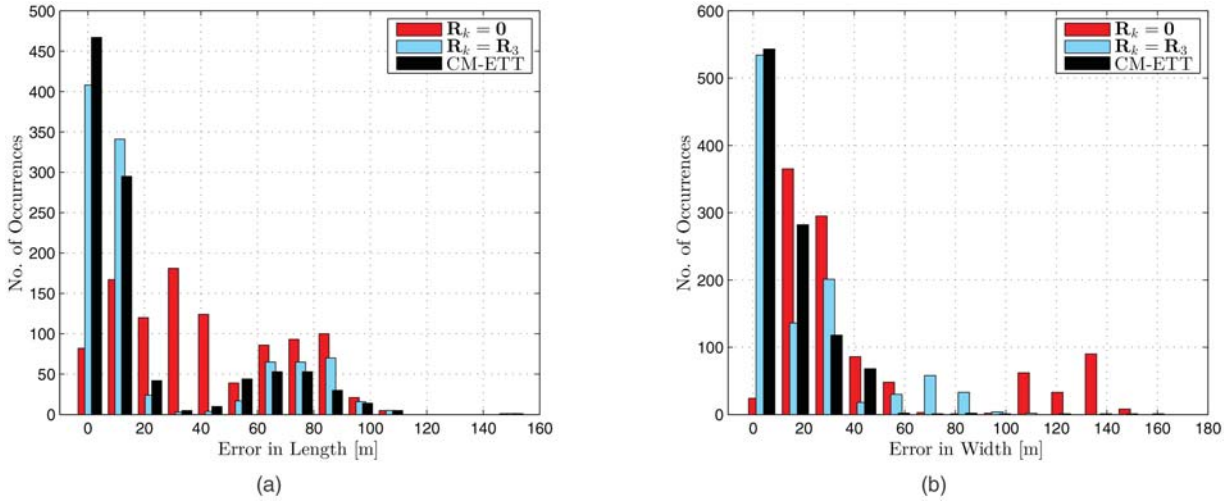

Fig. 12. Histograms of absolute errors in (a) length and (b) width for the $\mathbf{R}_k = \mathbf{0}$, the $\mathbf{R}_k = \mathbf{R}_3$, and the CM-ETT approach calculated on all the datasets.

are exploited as ground-truth. An example of the outcomes of the GGIW tracker with converted measurements model in the case of three very closely spaced targets is shown in Fig. 13. The tracking results are depicted in Fig. 14. They show the estimations for both kinematic and size parameters for all the targets in the scenario. Solid lines denote the values provided by the AIS, while dashed lines represent the estimations pro-

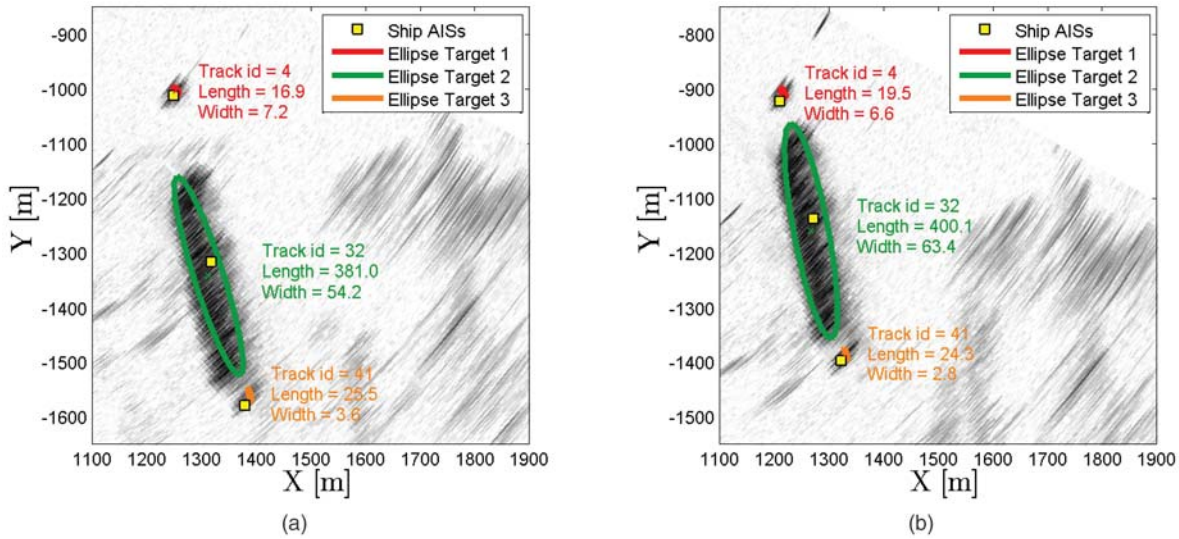

Fig. 13. Tracking of three spatially close targets that are part of the multiple extended target data set: (a) Frame 70; (b) Frame 90. AIS contacts are depicted with yellow square markers. The outcomes of the GGIW tracker with converted measurements model are indicated with colored ellipses.

TABLE VI
Parameter Settings GGIW-PHD

Parameter	Value	Specification
T_s	2 s	Sampling time
η_k	1.04	Forgetting factor
σ_a, σ_w	0.1 ms^{-2}, $\frac{0.1\pi}{180T_s}$ ms^{-2}	Kinematic noises
n	100	Extension uncertainty
τ	99	Temporal decay
ρ	1/4	Scaling parameter
σ_r, σ_θ	$\Delta r/2$, $\Delta\theta/2$ (see Tab. I)	Measurement noises
β_{FA}	$100/V(A)$ m^{-2}	Clutter density
P_D	0.99	Detection probability
P_S	0.99	Survival probability
$w_k^{(b)}$	10^{-2}	Birth weight
$m_k^{(b)}$	$\mathbf{0}_{5\times1}$	Birth mean
$P_k^{(b)}$	$\text{diag}\left(1,1,1,1,\frac{0.01\pi}{180T_s}\right)$	Birth covariance
$\alpha_k^{(b)}$, $\beta_k^{(b)}$	0.04, 0.008	Birth rate
$v_k^{(b)}$, $V_k^{(b)}$	120, $0.01\mathbf{I}_d$	Birth extension
$\bar{w}_0$	0.5	Extraction threshold
T	10^{-3}	Pruning threshold
U	25	Merging threshold
$\bar{w}_1$, $\bar{w}_2$, $\bar{w}_3$	1.1, 1, 0.8	Weight thresholds

vided by the GGIW tracker. The proposed approach reaches overall good performance. More specifically, we can appreciate only a small displacement between AIS information and the tracker's position estimation due to the fact that our approach estimates the center of the ellipse that represents the target (i.e. the ship), while the AIS returns the position of the transponder located on-board (usually not the ellipse's center). A further remark is related to the size estimation. Thanks to the usage of the proposed model, the tracker is able to compensate the usual bias in the size estimation with respect to the AIS values mainly due to the non-idealities of the acquisition system (i.e. the width of the radar antenna pattern's main lobe).

Regarding to the performance metrics, the TA indexes confirm the previous analysis. Indeed, Tab. VII shows limited errors. Average errors are 30.7 m and 0.69 ms^{-1} that are due to the discrepancy between the information provided by the radar and the one that the AIS is able to provide. Average errors for the size estimation are 19.7 m in length and 6.9 m in width and can be considered limited for the ships under test (we have ships hundreds meter long and an obscuration phenomena that affects the size estimation of the ship with maritime mobile service identity (MMSI) equal to 351361000 and increases the ϵ^{len} and the ϵ^{wid}).

The ToT is always very high (except for the ship with MMSI = 247031200, which is on the border of the surveillance area and could be not properly detected for some frames and the ship with MMSI = 247222500 that is a pilot boat and is often shadowed by or merged with the container ship with MMSI = 351361000). The overall ToT is 85%, see Tab. VII. Furthermore, the TF is almost ideal (with average values equal to 1.20). The small reduction of this index is only due to the obscuration phenomena for the container ship with MMSI = 351361000. Indeed, for about 40 frames, the passengers ship with MMSI equal to 255803790 interposed between the container ship and the radar causing a fragmentation of the container ship track for few frames and a reduction of the size estimation for that period. Finally, the FAR index is about $6.7 \cdot 10^{-7}$ $\text{s}^{-1}\text{m}^{-2}$. Furthermore, it is worth pointing out that the most of the false alarms are due to signal leakages in the electronics, buoys, and ghosts (coming from the radar antenna pattern's secondary lobes).

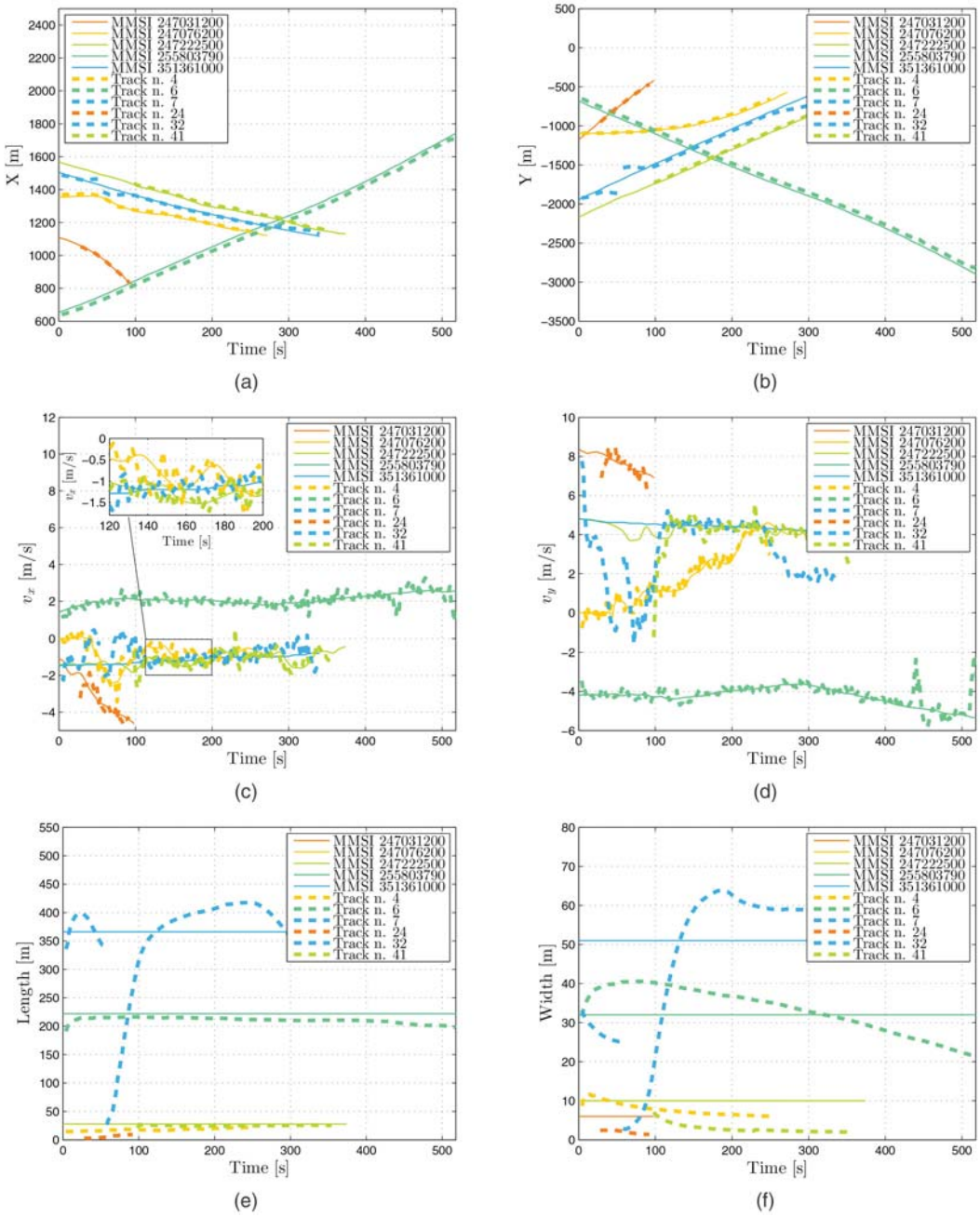

Fig. 14. Dashed lines represent tracks estimated by the GGIW tracker, while solid lines are used to depict AIS contacts. The association between GGIW estimated tracks and AIS tracks is indicated with different colors.

TABLE VII
Tracking Metrics

MMSI Ship	247031200	247076200	247222500	255803790	351361000	Average Results
ϵ^{pos} [m]	5.05	14.3	20.1	51.6	62.7	30.7
ϵ^{vel} [ms^{-1}]	0.52	0.41	0.49	0.33	1.70	0.69
ϵ^{len} [m]	22.2	9.8	2.9	11.2	52.4	19.7
ϵ^{wid} [m]	4.0	2.4	7.2	5.2	15.8	6.9
ToT	0.66	0.91	0.69	0.99	0.98	0.85
N^{TF}	1.00	1.00	1.00	1.00	2.00	1.20
FAR [m^{-2}s^{-1}]	$6.7 \cdot 10^{-7}$					

VII. CONCLUSIONS AND FUTURE DEVELOPMENTS

A maritime-surveillance system based on an X-band marine radar has been presented. The ability to estimate the targets' positions, velocities, and sizes using extended target tracking approaches relying upon random matrices has been evaluated. Standard and unbiased models have been proposed to properly take into account the radar's measurement noise. The validation has been conducted on both simulated and real data acquired by an X-band marine radar node installed in the Gulf of La Spezia, Italy. The integration of the proposed model into the gamma Gaussian inverse Wishart probability hypothesis density tracker has also been provided and tested on real data. Although comparable performance on the estimation of kinematic parameters has been pointed out, the experimental analysis confirms the ability of the proposed approach to better estimate the targets' size with respect to the approaches in [25] and [12], thanks to the use of proper models of the radar's measurement noise. Average gains up to 70% for the targets' width estimation accuracy and 65% for the length are observed on real data.

Future developments are devoted to the integration of the converted measurements model in other extended target tracking frameworks, such as the random hypersurface one, enabling a fair comparison among the different frameworks to track extended targets using polar/Cartesian coordinate conversion.

REFERENCES

[1] *Safety of Life at Sea (SOLAS) Convention*.
Chapter V, Regulation 19.

[2] D. Angelova and L. Mihaylova
Extended object tracking using Monte Carlo methods,
IEEE Transactions on Signal Processing, vol. 56, no. 2, pp. 825–832, Feb. 2008.

[3] Y. Bar-Shalom, P. Willett, and X. Tian
Tracking and Data Fusion: A Handbook of Algorithms.
Storrs, CT: YBS Publishing, Apr. 2011.

[4] M. Baum, M. Feldmann, D. Fränken, U. D. Hanebeck, and J. W. Koch
Extended object and group tracking: A comparison of random matrices and random hypersurface models,
in *Proceedings of IEEE International Society of Information Fusion 7th Workshop Sensor Data Fusion*, Leipzig, Germany, Oct. 2010.

[5] M. Baum and U. D. Hanebeck
Extended object tracking with random hypersurface models,
IEEE Transactions on Aerospace and Electronic Systems, vol. 50, no. 1, pp. 149–159, Jan. 2014.

[6] M. Baum and U. Hanebeck
Shape tracking of extended objects and group targets with star-convex RHMs,
in *14th International Conference on Information Fusion (FUSION)*, Jul. 2011.

[7] S. S. Blackman
Multiple hypothesis tracking for multiple target tracking,
IEEE Aerospace and Electronic Systems Magazine, vol. 19, no. 1, pp. 5–18, Jan. 2004.

[8] Y. Boers, H. Driessen, J. Torstensson, M. Trieb, R. Karlsson, and F. Gustafsson
Track before Detect algorithm for tracking extended targets,
IEE Proceedings Radar, Sonar and Navigation, vol. 153, no. 4, pp. 345–351, Aug. 2006.

[9] L. Bruno, P. Braca, J. Horstmann, and M. Vespe
Experimental evaluation of the range-Doppler coupling on HF surface wave radars,
IEEE Geoscience and Remote Sensing Letters, vol. 10, no. 4, pp. 850–854, Jul. 2013.

[10] M. Bruno
Bayesian methods for multiaspect target tracking in image sequences,
IEEE Transactions on Signal Processing, vol. 52, no. 7, pp. 1848–1861, Jul. 2004.

[11] B. Errasti-Alcala and P. Braca
Track before Detect algorithm for tracking extended targets applied to real-world data of X-band marine radar,
in *17th International Conference on Information Fusion (FUSION)*, Salamanca, Spain, Jul. 2014.

[12] M. Feldmann, D. Franken, and J. W. Koch
Tracking of extended objects and group targets using random matrices,
IEEE Transactions on Signal Processing, vol. 59, no. 4, pp. 1409–1420, Apr. 2011.

[13] K. Gilholm, S. Godsill, S. Maskell, and D. Salmond
Poisson models for extended target and group tracking,
in *Proceedings SPIE, Signal and Data Processing of Small Targets*, San Diego, CA, Aug. 2005, pp. 230–241.

[14] K. Gilholm and D. Salmond
Spatial distribution model for tracking extended objects,
IEE Proceedings Radar, Sonar and Navigation, vol. 152, no. 5, pp. 364–371, Oct. 2005.

[15] K. Granström, C. Lundquist, F. Gustafsson, and U. Orguner
Random set methods: Estimation of multiple extended objects,
IEEE Robotics and Automation Magazine, vol. 21, no. 2, pp. 73–82, Jun. 2014.

[16] K. Granström, A. Natale, P. Braca, G. Ludeno, and F. Serafino
PHD extended target tracking using an incoherent X-band radar: Preliminary real-world experimental results,
in *17th International Conference on Information Fusion (FUSION)*, Salamanca, Spain, Jul. 2014.

[17] ———
Gamma Gaussian inverse Wishart probability hypothesis density for extended target tracking using X-band marine radar data,
IEEE Transactions on Geoscience and Remote Sensing, vol. 53, no. 12, pp. 6617–6631, Jul. 2015.

[18] K. Granström and U. Orguner
Estimation and maintenance of measurement rates for multiple extended target tracking,
in *15th International Conference on Information Fusion (FUSION)*, Singapore, Jul. 2012.

[19] ———
A PHD filter for tracking multiple extended targets using random matrices,
IEEE Transactions on Signal Processing, vol. 60, no. 11, pp. 5657–5671, Nov. 2012.

[20] K. Granström, C. Lundquist, and O. Orguner
Extended target tracking using a Gaussian-mixture PHD filter,
IEEE Transactions on Aerospace and Electronic Systems, vol. 48, no. 4, pp. 3268–3286, Oct. 2012.

[21] K. Granström and O. Orguner
New prediction for extended targets with random matrices,
IEEE Transactions on Aerospace and Electronic Systems, vol. 50, no. 2, pp. 1577–1589, Apr. 2014.

[22] S. Grosdidier, A. Baussard, and A. Khenchaf
HFSW radar model: Simulation and measurement,
IEEE Transactions on Geoscience and Remote Sensing, vol. 48, no. 9, pp. 3539–3549, Sep. 2010.

[23] A. K. Jain, M. N. Murty, and P. J. Flynn
Data clustering: a review,
Association for Computing Machinery Computing Surveys, vol. 31, no. 3, pp. 264–323, Sep. 1999.

[24] T. Kirubarajan, Y. Bar-Shalom, and K. R. Pattipati
Multiassignment for tracking a large number of overlapping objects,
IEEE Transactions on Aerospace and Electronic Systems, vol. 37, no. 1, pp. 2–21, Jan. 2001.

[25] J. W. Koch
Bayesian approach to extended object and cluster tracking using random matrices,
IEEE Transactions on Aerospace and Electronic Systems, vol. 44, no. 3, pp. 1042–1059, Apr. 2008.

[26] J. W. Koch and M. Feldmann
Cluster tracking under kinematical constraints using random matrices,
Robotics and Autonomous Systems, vol. 57, no. 3, pp. 296–309, Mar. 2009.

[27] J. Lan and X. R. Li
Tracking of maneuvering non-ellipsoidal extended object or target group using random matrix,
IEEE Transactions on Signal Processing, vol. 62, no. 9, pp. 2450–2463, May 2014.

[28] R. Mahler
Multitarget Bayes filtering via first-order multitarget moments,
IEEE Transactions on Aerospace and Electronic Systems, vol. 39, no. 4, pp. 1152–1178, Jan. 2003.

[29] ———
Statistical Multisource-Multitarget Information Fusion.
Artech House, 2007.

[30] ———
PHD filters for nonstandard targets, I: Extended targets,
in *12th International Conference on Information Fusion (FUSION)*, Seattle, WA, Jul. 2009, pp. 915–921.

[31] S. Maresca, P. Braca, J. Horstmann, and R. Grasso
Maritime surveillance using multiple high-frequency surface-wave radars,
IEEE Transactions on Geoscience and Remote Sensing, vol. 52, no. 8, pp. 5056–5071, Aug. 2014.

[32] L. Mihaylova, A. Y. Carmi, F. Septier, A. Gning, S. K. Pang, and S. Godsill
Overview of Bayesian sequential Monte Carlo methods for group and extended object tracking,
Digital Signal Processing, vol. 25, pp. 1–16, Feb. 2014.

[33] U. Orguner
A variational measurement update for extended target tracking with random matrices,
IEEE Transactions on Signal Processing, vol. 60, no. 7, pp. 3827–3834, Jul. 2012.

[34] S. K. Pang, J. Li, and S. Godsill
Detection and tracking of coordinated groups,
IEEE Transactions on Aerospace and Electronic Systems, vol. 47, no. 1, pp. 472–502, Jan. 2011.

[35] S. Reuter and K. Dietmayer
Pedestrian tracking using random finite sets,
in *14th International Conference on Information Fusion (FUSION)*, Jul. 2011.

[36] H. Rohling
Radar CFAR thresholding in clutter and multiple target situations,
IEEE Transactions on Aerospace and Electronic Systems, vol. AES-19, no. 4, pp. 608–621, Jul. 1983.

[37] K. Romeo, P. Willett, and Y. Bar-Shalom
Particle filter tracking for banana and contact lens problems,
IEEE Transactions on Aerospace and Electronic Systems, vol. 51, no. 2, pp. 1098–1110, Apr. 2015.

[38] M. I. Skolnik
Radar handbook.
McGraw-Hill, Incorporated, 1970.

[39] L. Sun, X. R. Li, and L. J.
Modeling of extended objects based on support functions and extended Gaussian images for target tracking,
IEEE Transactions on Aerospace and Electronic Systems, vol. 50, no. 4, pp. 3021–3035, Oct. 2014.

[40] G. Vivone, P. Braca, K. Granström, A. Natale, and J. Chanussot
Converted measurements random matrix approach to extended target tracking using X-band marine radar data,
in *18th International Conference on Information Fusion (FUSION)*, 2015.

[41] G. Vivone, P. Braca, and J. Horstmann
Knowledge-based multi-target ship tracking for HF surface wave radar systems,
IEEE Transactions on Geoscience and Remote Sensing, vol. 53, no. 7, pp. 3931–3949, Jul. 2015.

[42] B.-N. Vo and W.-K. Ma
The Gaussian mixture probability hypothesis density filter,
IEEE Transactions on Signal Processing, vol. 54, no. 11, pp. 4091–4104, Nov. 2006.

[43] B.-N. Vo, S. Singh, and A. Doucet
Sequential Monte Carlo methods for multitarget filtering with random finite sets,
IEEE Transactions on Aerospace and Electronic Systems, vol. 41, no. 4, pp. 1224–1245, Oct. 2005.

[44] D. Wehner
High resolution radar.
Artech House, 1987.

[45] M. Wieneke and J. W. Koch
Probabilistic tracking of multiple extended targets using random matrices,
in *Proceedings SPIE, Signal and Data Processing of Small Targets*, Orlando, FL, Apr. 2010.

[46] ———
A PMHT approach for extended objects and object groups,
IEEE Transactions on Aerospace and Electronic Systems, vol. 48, no. 3, pp. 2349–2370, Jul. 2012.

Gemine Vivone received the B.Sc. (summa cum laude), the M.Sc. (summa cum laude), and the Ph.D. (highest rank) degrees in information engineering from the University of Salerno, Salerno, Italy, in 2008, 2011, and 2014, respectively. He is currently a Scientist at the North Atlantic Treaty Organization (NATO) Science & Technology Organization (STO) Centre for Maritime Research and Experimentation (CMRE), La Spezia, Italy. In 2014, he joined the NATO STO CMRE, La Spezia, Italy as a Research Fellow. In 2013, he was as a Visiting Scholar with Grenoble Institute of Technology (INPG), Grenoble, France, conducting his research at the Laboratoire Grenoblois de l'Image, de la Parole, du Signal et de l'Automatique GIPSA-Lab. In 2012, he was a Visiting Researcher with the NATO Undersea Research Centre, La Spezia, Italy. His main research interests focus on statistical signal processing, detection of remotely sensed images, data fusion, and tracking algorithms. Dr. Vivone serves as a Referee for several journals, such as *IEEE Transactions on Geoscience and Remote Sensing*, *IEEE Journal of Selected Topics in Applied Earth Observations and Remote Sensing*, and *IEEE Geoscience and Remote Sensing Letters*. Dr. Vivone was the recipient of the Symposium Best Paper Award at the IEEE International Geoscience and Remote Sensing Symposium (IGARSS) 2015.

Paolo Braca received the Laurea degree (summa cum laude) in electronic engineering, and the Ph.D. degree (highest rank) in information engineering from the University of Salerno, Italy, in 2006 and 2010, respectively. In 2009, he was a Visiting Scholar with the Department of Electrical and Computer Engineering, University of Connecticut, Storrs, CT, USA. In 2010–2011, he was a Postdoctoral Associate with the University of Salerno, Italy.

In 2011, he joined the NATO Science & Technology Organization Centre for Maritime Research and Experimentation (CMRE) as a Scientist with the Research Department.

Dr. Braca conducts research in the general area of statistical signal processing with emphasis on detection and estimation theory, wireless sensor network, multi-agent algorithms, target tracking and data fusion, adaptation and learning over graphs, distributed radar (sonar) processing.

He is coauthor of more than 70 publications in international scientific journals and conference proceedings. Dr. Braca serves as an Associate Editor of *IEEE Transactions on Signal Processing*, *IEEE Transactions on Aerospace and Electronic Systems*, *IEEE Signal Processing Magazine* (E-Newsletter), *ISIF Journal of Advances in Information Fusion*, and *EURASIP Journal on Advances in Signal Processing*. He is in the Technical Committee of the major international conferences in the field of signal processing and data fusion. He was the recipient of the Best Student Paper Award (first runner-up) at the 12th International Conference on Information Fusion in 2009.

Karl Granström (M'08) is a postdoctoral research fellow at the Department of Signals and Systems, Chalmers University of Technology, Gothenburg, Sweden. He received the M.Sc. degree in Applied Physics and Electrical Engineering in May 2008, and the Ph.D. degree in Automatic Control in November 2012, both from Linköping University, Sweden. He previously held postdoctoral positions at the Department of Electrical and Computer Engineering at University of Connecticut, USA, from September 2014 to August 2015, and at the Department of Electrical Engineering of Linköping University from December 2012 to August 2014. His research interests include estimation theory, multiple model estimation, sensor fusion and target tracking, especially for extended targets. He has received paper awards at the Fusion 2011 and Fusion 2012 conferences.

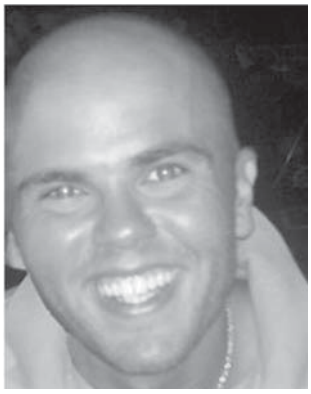

Antonio Natale was born in Naples, Italy, on July 3, 1982. He received the B.S. and M.S. degrees (both cum laude) in telecommunication engineering and the Ph.D. degree from the University of Naples Federico II, Naples, in 2005, 2008, and 2012, respectively. In 2011, he was a Visiting Scientist with the Surrey Space Centre, University of Surrey, Surrey, U.K. In that period, he was also the Principal Researcher for the project "Applications for S-band SAR," which was funded by EADS Astrium Ltd. He is currently a Research Fellow with the Institute for Electromagnetic Sensing of the Environment (IREA) of the Italian National Research Council (CNR), Naples. In 2013, he spent a period at the NATO Centre for Maritime Research and Experimentation (CMRE), La Spezia, Italy, as a Visiting Scientist to develop target detection and tracking strategies from high-resolution radar data. His research interests include remote sensing, the modeling of electromagnetic scattering from natural surfaces, signal processing, and the estimation of parameters from radar data. Dr. Natale received the 2009 IEEE Geoscience and Remote Sensing South Italy Chapter Prize for the best Italian thesis in remote sensing discussed in 2008. Moreover, he was the recipient of the 2009 S. A. Schelkunoff Transactions Prize Paper Award from the IEEE Antennas and Propagation Society, for the best paper published in 2008 on the *IEEE Transactions on Antennas and Propagation*.

Jocelyn Chanussot (M'04–SM'04–F'12) received the M.Sc. degree in electrical engineering from the Grenoble Institute of Technology (Grenoble INP), Grenoble, France, in 1995, and the Ph.D. degree from Savoie University, Annecy, France, in 1998. In 1999, he was with the Geography Imagery Perception Laboratory for the Delegation Generale de l'Armement. Since 1999, he has been with Grenoble INP, where he was an Assistant Professor from 1999 to 2005, an Associate Professor from 2005 to 2007, and is currently a Professor of Signal and Image Processing. He is conducting his research at the Grenoble Images Speech Signals and Automatics Laboratory. His research interests include image analysis, multicomponent image processing, nonlinear filtering, and data fusion in remote sensing. He has been a Visiting Scholar with Stanford University (USA), KTH (Sweden), and NUS (Singapore). Since 2013, he has been an Adjunct Professor with the University of Iceland. From 2015 to 2017, he is a Visiting Professor at the University of California, Los Angeles. He was the Founding President of the IEEE Geoscience and Remote Sensing French Chapter (2007–2010), which received the 2010 IEEE GRS-S Chapter Excellence Award. He was a co-recipient of the NORSIG 2006 Best Student Paper Award, the IEEE GRSS 2011 and 2015 Symposium Best Paper Award, the IEEE GRSS 2012 Transactions Prize Paper Award, and the IEEE GRSS 2013 Highest Impact Paper Award. He was a member of the IEEE Geoscience and Remote Sensing Society AdCom (2009–2010), in charge of membership development. He was the General Chair of the first IEEE GRSS Workshop on Hyperspectral Image and Signal Processing, Evolution in Remote sensing. He was the Chair (2009–2011) and Co-Chair of the GRS Data Fusion Technical Committee (2005–2008). He was a member of the Machine Learning for Signal Processing Technical Committee of the IEEE Signal Processing Society (2006–2008) and the Program Chair of the IEEE International Workshop on Machine Learning for Signal Processing, (2009). He was an Associate Editor of the *IEEE Geoscience and Remote Sensing Letters* (2005–2007) and *Pattern Recognition* (2006–2008). Since 2007, he has been an Associate Editor of the *IEEE Transactions on Geoscience and Remote Sensing*. He was the Editor-in-Chief of the *IEEE Journal of Selected Topics in Applied Earth Observations and Remote Sensing* (2011–2015). In 2013, he was a Guest Editor of the *Proceedings of the IEEE* and the *IEEE Signal Processing Magazine* in 2014. He is a member of the Institut Universitaire de France (2012–2017).